Environmental reconstruction of Ain el Beida (Atlantic site of the Rifian Corridor, Morocco) during the first stages of the Messinian Salinity Crisis using benthic foraminifera

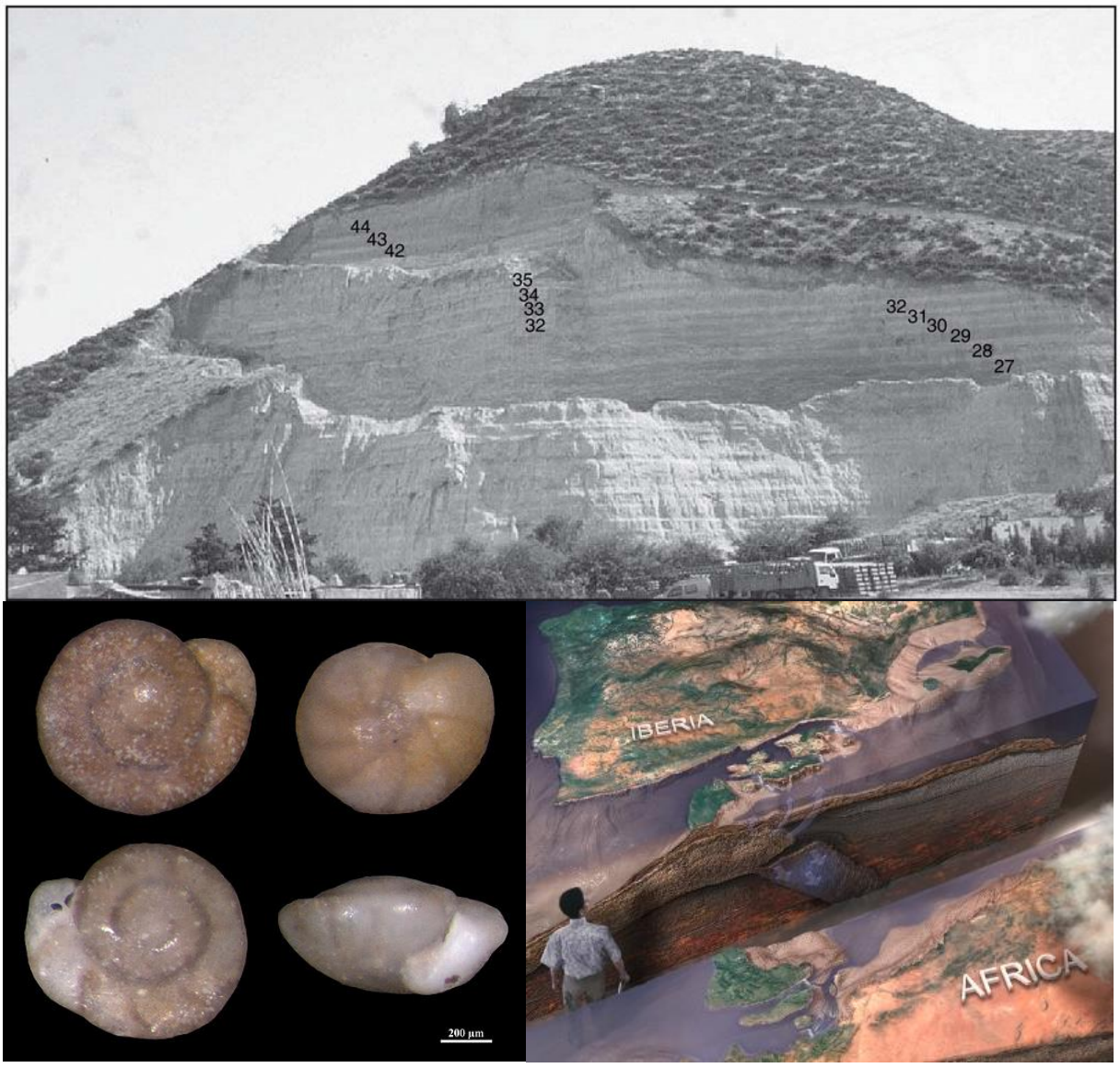

Master thesis
W.C. van den Berg
3790118

Utrecht University, 13-04-2017
Supervisor 1: dr. F.J. Hilgen
Supervisor 2: dr. T.J. Kouwenhoven

Abstract

Studies show that water exchange between the Mediterranean Sea and Atlantic Ocean must have occurred during the first stage of the Messinian Salinity Crisis (MSC). However, the scale and location of this exchange is poorly understood. Benthic foraminiferal assemblages of the Ain el Beida section are therefore studied to expose the bathymetric history and environmental conditions on the Atlantic side of the Rifian Corridor during the first stages of the MSC. In addition, studies suggest that the cyclic alternations of red and light beige marls of the Ain el Beida section are related to the alternations of sapropels and marls of Mediterranean sections. The benthic foraminiferal assemblages of this study are used to evaluate this relation. Benthic foraminifera are used as proxy because they accurately record changes in the environment. The benthic assemblages show a clear astronomical signal related to the cyclic alternations of red and light beige marls. They indicate lowered oxygen levels and enhanced organic flux during red marl formation. The light beige marls are associated with reoxygenation. The red marls are linked to Mediterranean sapropels, but the reduction in oxygen levels was not as extreme as during sapropel formation. The distribution of the species *U. pigmea* indicates coastal upwelling during red marl formation. The study demonstrates that the perceived reduction in vertical circulation during red marl formation is best explained by increased fluvial run-off and precipitation instead of Mediterranean outflow. The paleodepth reconstruction demonstrates a relatively deep and stable interval during the first stage of the MSC. A shallowing of 200-300 m occurred during the extreme second stage of the MSC. The benthic assemblages of the Ain el Beida do not show evidence for Mediterranean outflow during the first stages of the MSC. However, Mediterranean outflow to the Rifian Corridor during the first stage of the MSC cannot be excluded.

1. Introduction

During the Messinian stage of the Miocene epoch, the Mediterranean Sea witnessed extreme environmental changes, referred to as the Messinian Salinity Crisis (MSC). The crisis is dated from 5.97-5.33 Ma (Krijgsman et al., 1999a,b; Manzi et al., 2013). The MSC was caused by the near-complete closure of the connections between the Mediterranean Sea and the Atlantic Ocean. These connections are the Betic Corridor through Spain and the Rifian Corridor through Morocco. They are visualized in Figure 1. The isolation decreased the supply of Atlantic waters to the Mediterranean, resulting in hypersaline conditions and eventually extensive deposition of evaporites (Ogniben, 1957; Hsü, 1973; Ryan et al., 1973; Ryan, 2009).

However, the isolation during the first stage of the MSC (5.97-5.60 Ma) was not complete. Studies on the Lower Evaporites of the first stage show that these evaporites required a continuous marine environment. Further isolation of the Mediterranean Sea occurred after the deposition of the Lower Evaporites during the second, more extreme stage of the MSC (5.60-5.55 Ma) (Krijgsman et al., 1999b; Hilgen et al., 2007). Although exchange between Mediterranean and Atlantic waters must have occurred during the first stage, little is known about the scale and location of the outflow of Mediterranean waters (Flecker et al., 2015).

Furthermore, sedimentary sections located in the Atlantic side of the Rifian Corridor display cyclic alternations in lithology that show similar characteristics to the alternations of sapropels and homogenous marls in Mediterranean sections. Multiple proxy signals suggest a close relation (Hilgen et al., 2000; van der Laan et al., 2012). In contrast to Mediterranean sections, little has been published about the environmental conditions during the depositional phase of the sections in the Rifian Corridor. Therefore, it is not clear under which environmental conditions the cyclic alternations of sections in the Rifian Corridor formed.

To investigate what factors controlled the environment of the Rifian Corridor during the first stages of the MSC, the possible influence of Mediterranean outflow and the mechanisms behind the cyclic alternations in lithology can be examined. The benthic foraminiferal assemblages of the Ain el Beida section are used for this project.

The Ain el Beida section is selected because it is located in the Atlantic side of the Rifian Corridor, connecting the Mediterranean Sea to the Atlantic Ocean. The section remained marine during the MSC, making it an excellent site to study benthic foraminiferal assemblages. Furthermore, the section displays cyclic alternations of red and light beige marls. Consequently, the relation with sapropels and homogeneous marls from Mediterranean sections can be studied. Moreover, little has been published about benthic assemblages in the Atlantic side of the gateway (Barbieri and Ori, 2000). The section has already been described stratigraphically and dated astronomically (Benson et al., 1995; Krijgsman et al., 2004; van der Laan et al., 2005). It shows a clear astronomical signal related to precession, eccentricity and obliquity (van der Laan et al., 2005).

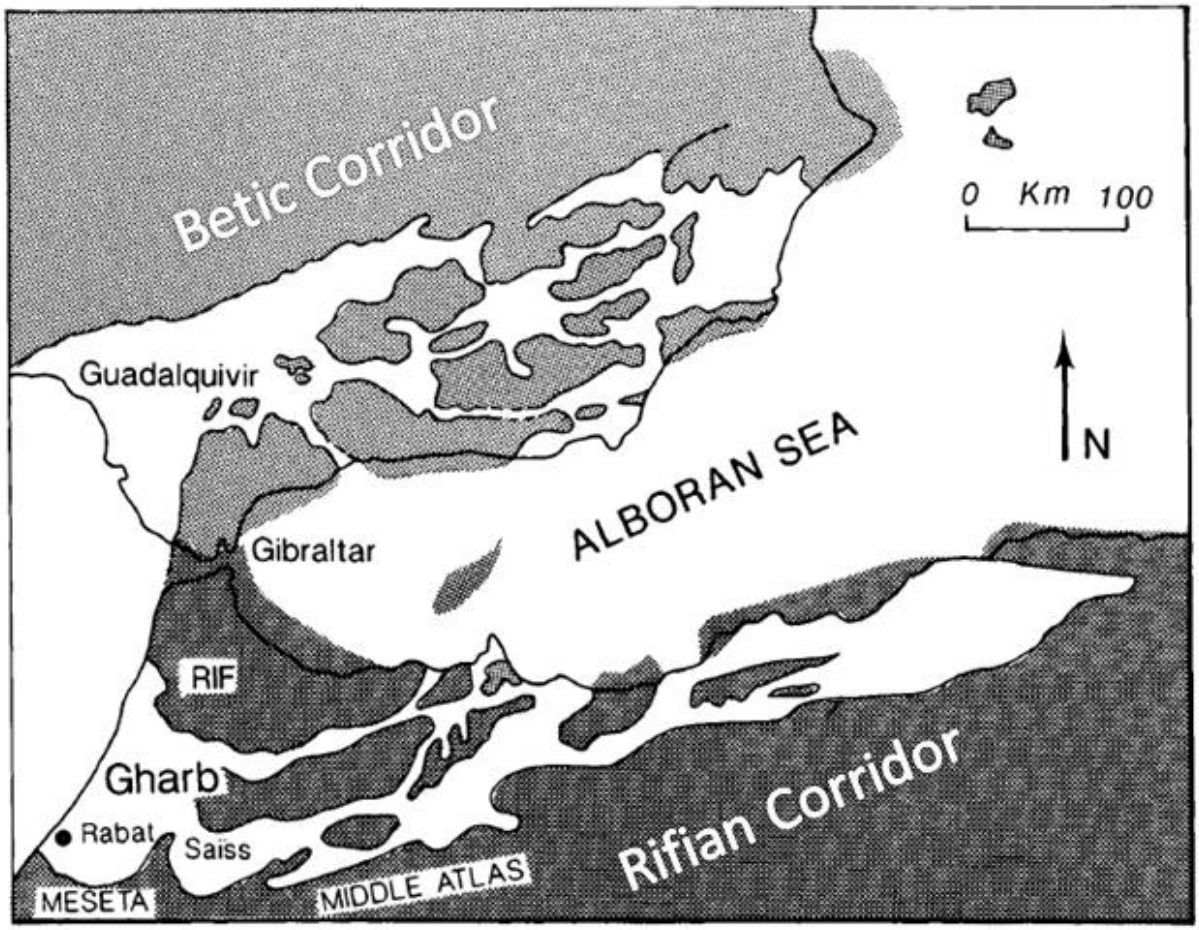

Fig. 1 – The Rifian Corridor (Morocco) and the Betic Corridor (Spain) during the Tortonian-Messinian boundary, before the onset of the MSC (modified after Esteban et al., 1996)

The rich diversity and extensive occurrence in marine sediments make benthic foraminifera an excellent proxy for reconstructing environment. They have been used to reconstruct bathymetry, salinity, oxygen levels and nutrient availability (van der Zwaan et al., 1990; Murray, 1991). However, these reconstructions are not without complications (van der Zwaan et al., 1999) and these will be addressed. Benthic foraminifera live on or within the ocean floor. The dense and salty Mediterranean outflowing waters are expected to sink on the Atlantic side of the Rifian Corridor. If present, they should influence the benthic ecosystem. The planktonic foraminiferal assemblages of the Ain el Beida section have already been studied by van der Laan et al. (2012). They will be compared to the results of this study.

The research objective is to obtain a detailed environmental reconstruction of the Atlantic side of the Rifian Corridor during first and second stage of the MSC (5.95-5.52 Ma). A comprehensive bathymetric reconstruction will be performed to investigate if changes in paleodepth influenced the exchange between the Atlantic Ocean and the Mediterranean Sea. Additional environmental factors such as oxygen concentration and organic flux will be reconstructed as well. The mechanisms controlling these environmental factors will be discussed to investigate which processes influenced the environmental changes in the Atlantic side of the Rifian Corridor. Consequently, these will be compared to the mechanisms controlling the environmental changes during the formation of Mediterranean sections.

2. Background

2.1 *Messinian Salinity Crisis*

The Messinian Salinity Crisis (MSC) has been a topic of many studies in the last 70 years. The first notion of a salinity crisis during the Late Miocene originated from onshore studies that demonstrated large scale deposits of evaporites. These studies on sections throughout the Mediterranean demonstrated a widespread hyposaline and hypersaline environment during the Late Miocene (Ogniben, 1957; Selli, 1960). The evaporites present in the Gessoso Solfifera formation in Sicily were attributed to the isolation of the Mediterranean Sea (Ogniben, 1957).

In the following decades the magnitude of the event was further demonstrated by the Deep Sea Drilling Project (DSDP) Leg 13, which recovered for the first time the top of the Upper Evaporite unit in the Mediterranean Sea (Hsü, 1972; Hsü, 1973; Ryan et al., 1973). This confirmed the hypothesis that the salinity crisis was a large-scale environmental event that affected the entire Mediterranean Sea. However, there was controversy about the depth of the basin and the waterdepth at which the evaporites were deposited. Consequently, 3 hypotheses were proposed about the origin of the evaporites: The 'deep–basin, deep-water', 'deep-basin, shallow-water' and 'shallow-basin, shallow-water' models. The overwhelming evidence for extensive erosion by rivers draining into the Mediterranean in the Late Miocene supports the 'deep-basin, shallow-water' hypothesis (Ryan, 1978; Clauzon, 1996; Maillard et al., 2006; see also Ryan, 2009 for an overview). Therefore it turned out that only the deep-basin shallow-water scenario, whereby the Mediterranean Sea transformed into a salt desert laying 1 km below the sea level of the Atlantic Ocean, could explain all the data obtained (Roveri et al., 2014). According to Ryan (2009) this salt desert was located more than 3km below the Atlantic Ocean. However, studies on the Lower Evaporites show that these evaporites require a continuous marine environment favouring a deep-water scenario for the early stages of the MSC. Isolation of the Mediterranean Sea and extensive erosion by rivers only occurred after the deposition of the Lower Evaporites (Krijgsman et al., 1999b; Hilgen et al., 2007; Flecker et al., 2015).

Another controversy has been and still is the cause of the MSC. It was proposed that either global glacio-eustatic sea level changes or regional tectonic activity between Africa and Iberia was the cause of the closure of the gateways resulting in isolation of the Mediterranean (Krijgsman et al. 1999a). A combination of both factors was considered to be possible as well. However, stable isotope analyses from the astronomically tuned Ain el Beida section showed that peak glacial stages post-date the deposition of the Mediterranean evaporites (Krijgsman et al., 2004). In addition, benthic $\delta^{18}O$ values of ODP Leg 162, Site 982 in the North Atlantic show no evidence for a glacio-eustatic cause of the closure (Hodell et al., 2001). Consequently, the closure was considered to be primarily the result of plate tectonic convergence of Africa and Iberia. In addition, subduction in the region of the Alborán Sea attributed to the closure (Flecker et al., 2015). A new high-resolution age model of Manzi et al. (2013) confirmed that the onset of the MSC was indeed preconditioned by tectonic activity. However, the timing indicates that the MSC was triggered by arid conditions in North Africa

and glacial conditions in the Northern Hemisphere as well. This reduced the hydrological exchange between the Atlantic Ocean and the Mediterranean Sea (Manzi et al., 2013).

The MSC is defined as the isolation of the Mediterranean Sea from the Atlantic Ocean and was dated from 5.97-5.33 Ma (Krijgsman et al., 1999a,b). This timespan has been established by use of astronomical tuning of sedimentary cycles of sections throughout the Mediterranean. A higher resolution revised age calibration based on the recognition of an extra gypsum cycle in the Perales section resulted in an age of the onset of the MSC of 5.971 Ma (Manzi et al., 2013). The isolation of the Mediterranean Sea during the MSC was probably not complete. The amount of salt that was deposited required additional hydrological exchange through gateways with major oceanic basins (presumably the Atlantic Ocean) during the first part of the MSC until at least 5.55 Ma (Flecker et al., 2015).

According to recent consensus models the MSC is divided into three stages. This model is based on integrated bio-, cyclo- and magnetostratigraphy as well as seismic stratigraphy from studies on onshore and offshore sections (Roveri et al., 2014). The first stage (5.97-5.60 Ma) is marked by the depositions of the Lower Evaporites. Integrated stratigraphy demonstrates 16 alternations of massive gypsum beds (1-35 m) and shales. The second stage (5.60-5.55 Ma) is the most extreme environmental stage. Massive deposition of halite occurred in Sicily, Calabria and Cyprus (Roveri et al., 2008). This stage is also marked by widespread erosion creating the Messinian Erosional Surface (MES). The glacials during this stage probably lowered sea level, creating deep canyons and probably causing further isolation of the Mediterranean Sea (Manzi et al., 2013). Stage 3 (5.55–5.33 Ma) is marked by the Upper Evaporites. Gypsum beds and clastic deposits mark a less extreme environment also known in literature as Lago-Mare. Brackish and freshwater flora and fauna indicate a dilution of surface waters (Roveri et al., 2014). The MSC ended with the Zanclean flood at 5.33 Ma Massive inflow and erosion by Atlantic waters probably created the present gateway at the Gibraltar Strait. The Mediterranean basin refilled rapidly with a sea level rise of meters per day (Garcia-Castellanos et al., 2009).

2.2. *Astronomical cyclicity*

Sections throughout the Mediterranean show a clear astronomical signal before and during the first stage of the MSC (Sierro et al., 1993; 2001; Krijgsman, 1999a,c; Hilgen and Krijgsman, 1999; Krijgsman et al., 2001, 2002; Raffi et al., 2003). The astronomical signal refers to a pattern that is the result of the cyclicity of the changes of Earth's orbit. This pattern is an interference of the precession cycle (~20 kyr) and the obliquity cycle (~40 kyr). Eccentricity (~100 kyr and ~400 kyr) acts as amplitude modulator for precession. The interference pattern is recorded through changes in colour reflectance, chemical composition, stable isotope ratios and microfossil assemblages. High-resolution age models of multiple sections are constructed by use of astronomical tuning. This allows correlation between the sections on a bed to bed basis (Krijgsman et al. 1999b). The cyclic alternations present in the sections are related to climatic changes. The precession signal (with eccentricity as amplitude modulator) largely controls regional climate change whereas the obliquity signal is related to glacial cyclicity (Hilgen et al., 2007).

The astronomical signal in Messinian pre-evaporitic sequences is very clear. The patterns of the sedimentary cycles show an outstanding fit to the interference pattern of precession, obliquity and eccentricity. Therefore, correlation between different sections is straightforward (Hilgen et al., 2007). The oldest Lower Evaporite of the MSC formed synchronously at an age of 5.98 Ma in all known basins (Krijgsman et al., 1999b). The alternations of gypsum and shales in the Lower Evaporites fit well with the precession cycle (Krijgsman et al., 2001). The deposits of the Upper Evaporites are marked with seven to eight sedimentary cycles. The amount of these cycles fit with the total number of precession peaks (Hilgen et al., 2007).

Sections in Atlantic basins close to the Mediterranean, such as the Ain el Beida section, show a very clear astronomical signal as well. Furthermore, during the timespan of the MSC these sections show sedimentary cycles that fit well with the interference pattern of precession and obliquity (Krijgsman et al., 2004).

2.3 *Mediterranean-Atlantic corridors*

Before the MSC there were two main gateways that allowed water exchange between the Mediterranean Sea and the Atlantic Ocean. These are the Betic Corridor in Spain and the Rifian Corridor in Morocco (Fig. 1) (Santisteban & Taberner, 1983; Benson et al., 1991 and see overview in Flecker et al., 2015). Many questions about the water exchange through these corridors are not yet resolved in detail (Flecker et al., 2015). However, the restriction of the corridors resulted in the isolation of the Mediterranean Sea leading to the extreme environments of the MSC. Considering the amount of evaporites deposited during the MSC , water exchange between the Mediterranean Sea and the Atlantic Ocean must have been present. The extensive halite deposits require additional water exchange to be explained. This means that the isolation of the Mediterranean Sea was not complete (Krijgsman et al., 1999b; Hilgen et al., 2007; Flecker et al., 2015). Because sedimentary successions were eroded because of tectonic uplift, the timing, duration and amount of water exchange during MSC is not fully known. Furthermore, it is not known through which of the corridor(s) the water exchange occurred during the MSC (Flecker et al., 2015).

Rifian Corridor

Exposures of the Rifian Corridor consist of multiple basins. The Taza–Guercif basin is located to the east of the corridor (Fig. 2). The oldest marine sediments in this basin are deposited approximately 8 Ma, probably marking the opening of the Rifian Corridor. Paleodepth reconstructions demonstrate a shallowing phase that began at 7.2 Ma This was primarily the result of tectonic activity with minor influence of glacio-eustatic sea level lowering. This resulted in the emergence of the basin at 6.0 Ma This was followed by continental sedimentation in the Taza–Guercif region (Krijgsman et al., 1999c). Another basin located to the west of the corridor is the Gharb basin (Fig. 2). During the MSC this remained a marine basin, connected to the Atlantic Ocean (Krijgsman et al., 2004). Several sections in this basin have been studied, including the Ain el Beida section.

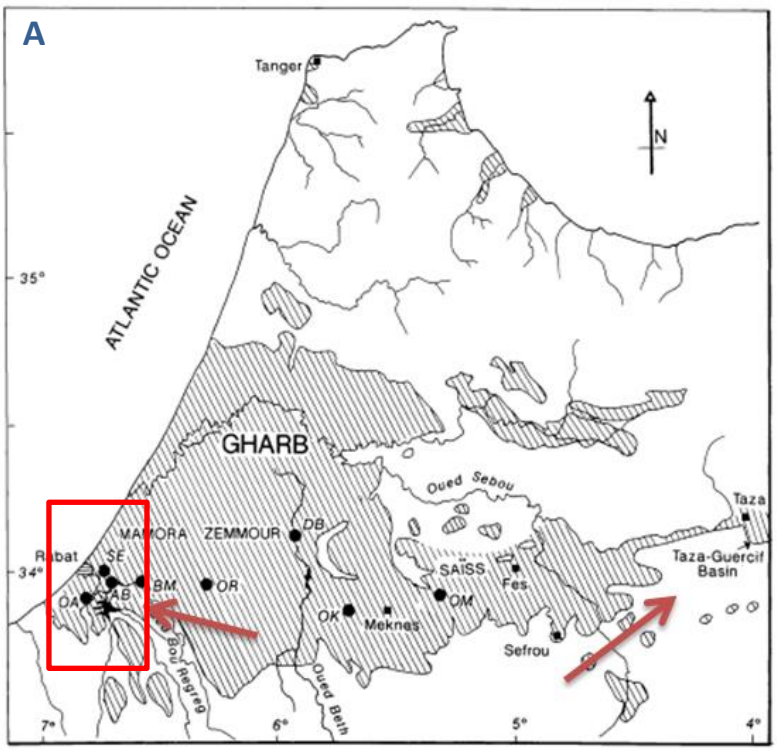

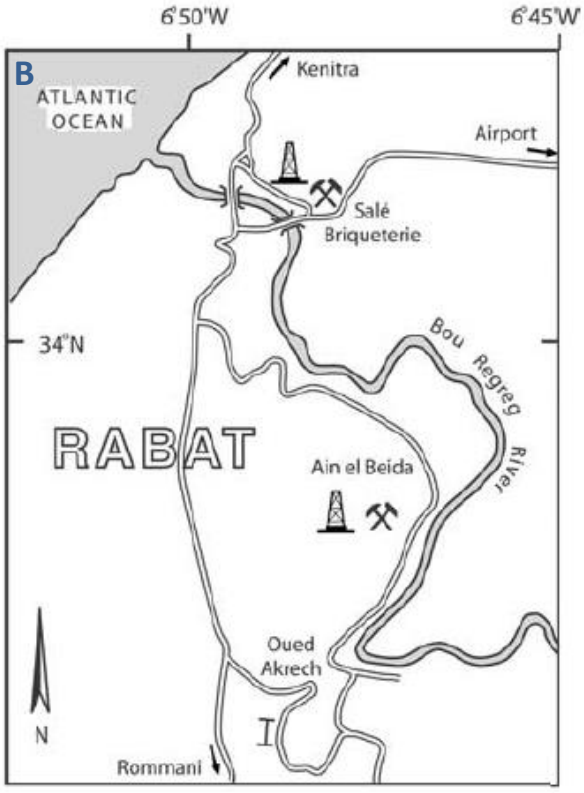

Fig. 2
A: The Gharb basin and the Taza-Guercif basin in Morocco. The Gharb basin is located to the west and contains several sections including the Ain el Beida (AB) section (left arrow) near Rabat. The Taza-Guercif basin is located to the east (right arrow). (Modified after Barbieri and Ori, 2000)
B: Closer view of the location of the Ain el Beida section (van der Laan et al., 2005)

2.4 *Ain el Beida section*

The Ain el Beida section consists of 44 cycles of light beige marls and reddish coloured marls. The layers are between 60-350 cm thick. The age model of the Ain el Beida section of the study of Krijgsman et al. (2004) is shown in Figure 3. The age model is constructed by use of astronomical tuning. The astronomical polarity time scale (APTS) as applied by Sierro et al. (2001) which includes nine major planktonic foraminiferal events and all magnetic reversals during the Messinian was used to define ages to the magnetic reversals and bio-events in the Ain el Beida section. These ages were then used for the age model, providing age control points that allow astronomical tuning. The solution of Laskar et al. (1993) was used for the tuning. Van der Laan et al. (2012) modified this age model using the solution of Laskar et al. (2004), but the differences in the control points were only minor (approximately 1 kyr). The age of the section ranges from 6.5-5.5 Ma

The alternations of red marls and light beige marls are strongly linked to the precession signal. During high amplitude precession minima, the red marls (in Figure 3 indicated as dark lithological units) tend to be darker and thicker. The interference with the eccentricity and obliquity signal modifies the darkness and thickness of the red marls. This is indicated in column E+T-P in Figure 3 where E is the eccentricity, T is the obliquity and P is the precession signal. Eccentricity and obliquity maxima result in a stronger expression of the red marls. High amplitude precession minima are associated with strong summer insolation maxima. During low amplitude precession minima, the red marls are lighter and thinner. Low amplitude precession minima are associated with reduced summer insolation maxima. Occasionally, there are no red marls present at all. At those times forcing was probably too low to enforce the formation of a red marl layer. This is the case for the low amplitude precession minima at approximately 5.6 Ma. This results in a relatively thick beige marl of cycle 41 that covers multiple precession cycles.

The obliquity signal is clearly present in the planktonic and benthic $\delta^{18}O$ signal of the Ain el Beida section (van der Laan et al., 2005). This signal is related to glacial and interglacial variation. The lag in the obliquity signal is probably the result of the growth of the ice sheets. The obliquity signal is present in the chemical composition and the assemblages of planktonic foraminifera and calcareous nannofossils as well, but in a lesser degree. They indicate warmer and wetter climates during interglacials. The obliquity signal is attributed to changes in Atlantic depressions, associated with a direct response to ice sheet development (van der Laan et al., 2012).

The clear imprint of the precession signal is probably the result of regional climate response to changes in precession (van der Laan et al., 2005). A study on the Ain el Beida section from van der Laan et al. (2012) shows that the red marls (precession minimum) correspond to relatively humid climate conditions. This is based on the Ti/Al ratio of the sediments. The assemblages of calcareous nannofossils and planktonic foraminifera demonstrate high sea surface temperatures during precession minima. In contrast, the light beige marls (precession maxima) correspond to relatively arid conditions and lower sea surface temperatures. In addition, during precession maxima there is a relatively high productivity of planktonic foraminifers and calcareous nannofossils. These climate variations in Northwest Africa are presumably linked to the Atlantic system (van der Laan et al., 2012). This is in contrast to sections in the Mediterranean. The different environmental conditions leading to the alternations of sapropels and marls in Mediterranean sections are traditionally linked to the African Monsoon system, of which the strength is controlled by precession (Rossignol-Strick, 1985; Larrasoaña et al., 2003; Tuenter et al., 2003).

The African monsoon is strengthened during precession minima because of the enhanced insolation. This leads to increased precipitation in Northern Africa. The relatively high precipitation results in an increase in freshwater run-off by rivers. In the eastern Mediterranean this will be mainly the Nile River. This freshwater is significantly lower in density than the salt waters of the Mediterranean Sea, causing stratified waters and decreasing the vertical circulation significantly. This results in the formation of a sapropel. Stronger freshwater run-off results in a stronger expression of sapropels. During precession maxima the freshwater run-off is reduced and vertical circulation is restored. Therefore no sapropels will form (Rossignol-Strick, 1985; Larrasoaña et al., 2003). However, increased precipitation over the Mediterranean region and run-off from European rivers during

enhanced seasonality (i.e. precession minima and obliquity maxima) are also linked to sapropel formation (Meijer and Tuenter, 2007).

The red marls of the Ain el Beida section share characteristics with the sapropels of Mediterranean sections. The astronomical tuning of the sections links sapropels to red marls (Hilgen et al., 2000). Multiple proxy signals, such as planktonic $\delta^{18}O$, planktonic foraminiferal events and SST proxies suggest similar environmental conditions (van der Laan et al., 2012).

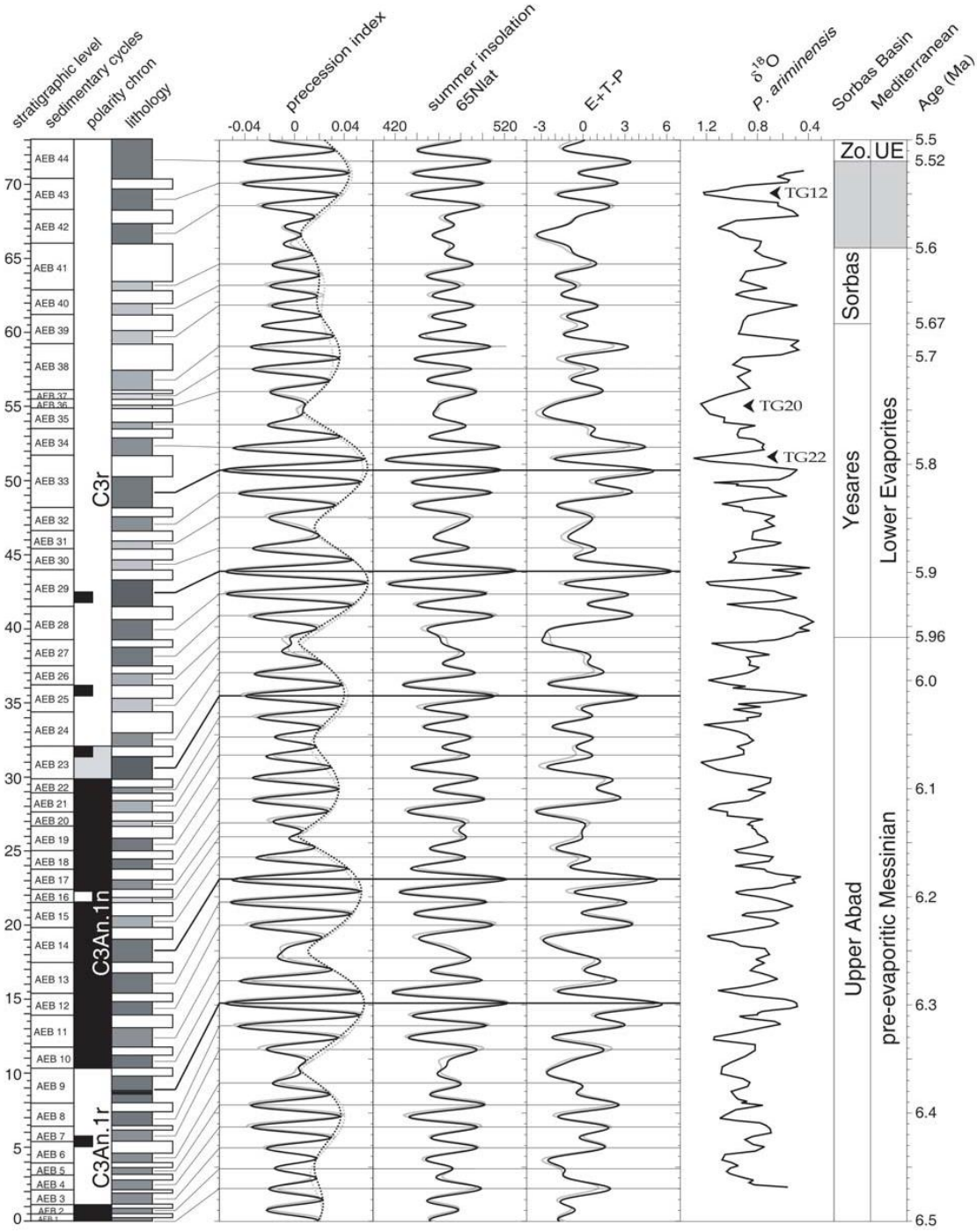

Fig. 3 – Age model of the Ain el Beida section (Krijgsman et al., 2004). Ages are the result of astronomical tuning of the 44 layers of light beige marls and red marls. Magneto- and biostratigraphy were used for the tuning.

2.5 *Benthic foraminiferal studies*

Benthic foraminiferal assemblages are used in studies as a proxy to reconstruct environmental changes (van der Zwaan et al., 1999). Foraminifera are protists; single celled eukaryotes. In contrast to planktonic foraminifera that float in the water column, benthic foraminifera live on the seafloor or within the seafloor sediments. The oldest fossils of foraminifera are exclusively agglutinated benthic taxa (test constructed of sediment particles). They have been found in Early Cambrian sediments (Pawlowski et al., 2003).

The evolution of early foraminifera is traditionally viewed as a gradual process in which primitive unilocular (single-chambered) organic-walled taxa developed agglutinated walls and evolved into multilocular (multi-chambered) forms (Hansen, 1979). The fossil evidence suggests that foraminifera originated during the Cambrian explosion alongside other skeletonized organisms. However, molecular phylogenetic studies suggest that non-skeletonized foraminifera appeared a billion years before the Cambrian explosion and that they originated from a Cercozoan ancestor (Langer et al., 1999). These Precambrian 'naked' ancestral taxa are not found in the fossil record because they lack any hard parts that can fossilize. The combination of fossil and molecular data strongly indicates that the Cambrian appearance of skeletonized foraminifera is preceded by a large radiation of non-skeletonized unilocular species. They gave rise to a wide variety of morphological forms which are present today in marine and freshwater environments. They are classified as Monothalamida. Another radiation is observed in the Cambrian which led to the development of multilocular agglutinated and calcareous tests (Pawlowski et al., 2003). These are classified as Polythalamida and are very diverse in morphology.

Benthic foraminifers are very divers, occur ubiquitously in marine sediments and react to environmental changes. Therefore they are potentially an excellent proxy for environmental reconstruction. The tests of benthic foraminifera are used in geochemistry for various purposes. Oxygen and carbon isotopes analyses ($\delta^{18}O$ and $\delta^{13}C$) on the calcite tests have been widely implemented to address a large range of questions regarding the history of the Earth's oceans and climate (Ravelo and Hillaire-Marcel, 2007). Element ratios, such as Mg/Ca and Sr/Ca, are used to reconstruct deep-sea temperatures and global weathering fluxes (Lear et al., 2000; Lear et al., 2003). Benthic foraminiferal assemblages are used as proxy to reconstruct bathymetry, salinity, oxygen levels and nutrient availability. In addition, the species diversity, the benthic foraminifera accumulation rate (BFAR) and the ratio between planktonic and benthic foraminifera (P/B ratio) are used for environmental reconstruction as well (van der Zwaan et al., 1990; Murray, 1991).

Oxygen levels and nutrient availability are the main drivers and limitations behind the abundance and diversity of benthic foraminiferal species (van der Zwaan et al, 1999). This is also apparent from the TROX model (Jorissen et al., 1995). This model, presented in Figure 4, shows that the benthic foraminiferal community is mainly determined by the combination of oxygen and organic flux. If this model is applied to a transect of shallow to deep water, it shows that in shallow waters oxygen is the most important parameter. This is because the organic flux is very high in these eutrophic shallow waters and therefore all the oxygen is consumed in the upper part of the sediment. This will result in benthic foraminiferal biomass loss in the anoxic deeper sediments. At intermediate waterdepths the organic flux and thus the oxygen consumption is decreased and therefore oxygen can penetrate deeper into the sediments resulting in more benthic foraminifera. At the deepest part of the ocean the organ flux is very low and is therefore the limiting factor. All the organic matter is already consumed in the upper part of the sediment preventing benthic foraminifera to live in the deeper sediments (van der Zwaan et al, 1999). The model also shows that stressed environments alter the habitats of species. When oxygen levels are reduced significantly, typical deep infaunal species will occupy the upper sediments, which are normally occupied by epifaunal species. These epifaunal species disappear due to the stressed environments. In contrast, in oxyphilic environments, deep infaunal species may not be present at all. This is because all the organic matter is consumed by the epifaunal species in the upper sediments (Jorissen et al., 1995).

The species diversity, also referred to as α index or Shannon (H) index, is the sum of all fractions of the species (*pi*) present in the sample:

$$H = -\sum_{i=1}^{n} pi \ln pi$$

(Spellerberg and Fedor, 2003)

It corrects for differences in sample size and single occurrences. The diversity generally decreases in stressed environments (Murray, 1991; van der Zwaan et al., 1999). This is because oxyphilic taxa will disappear in low-oxygen concentration environments.

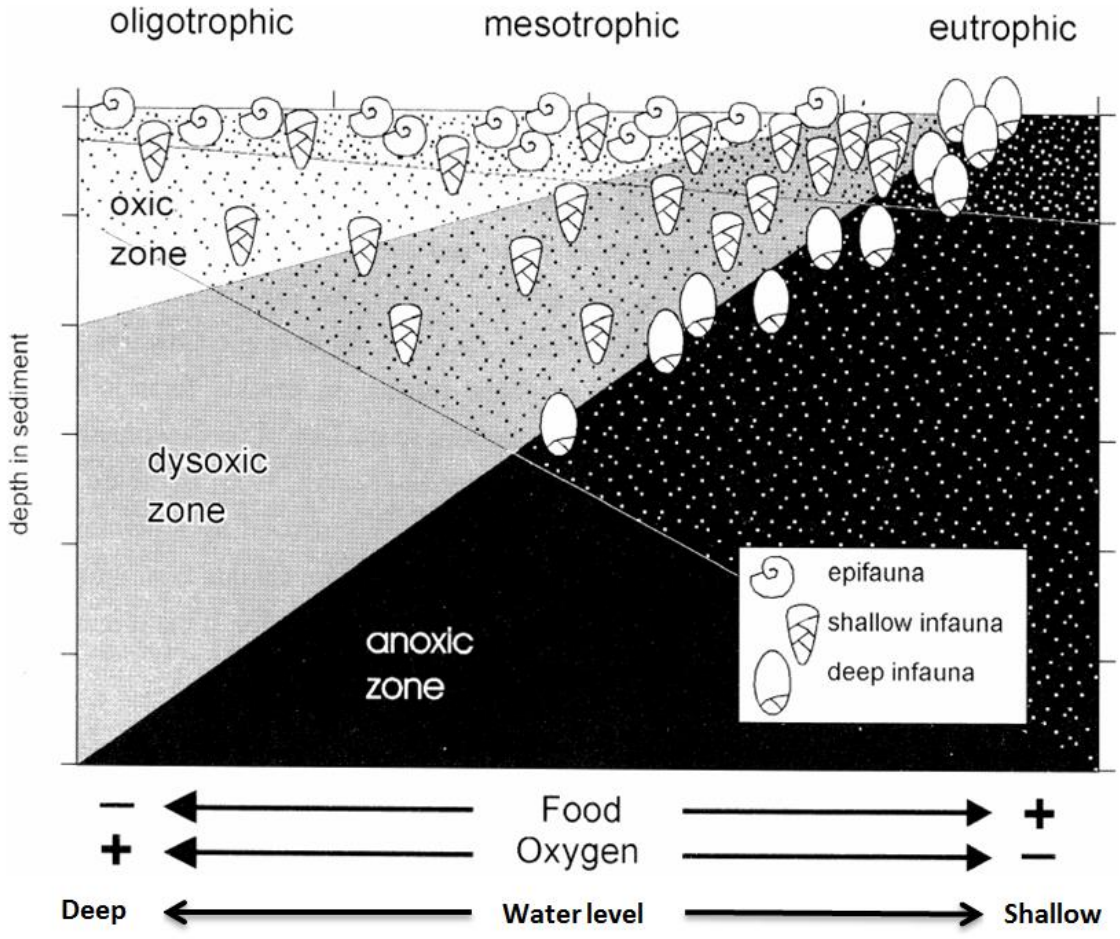

Fig. 4 – The TROX model, modified after Jorissen et al. (1995)

Studies on living benthic foraminifera show that the benthic foraminiferal accumulation rate (BFAR) is related to the primary productivity at the surface of the ocean (Herguera, 1992). When this productivity is high there will be a large organic flux to the sea floor. This will supply organics to the benthic foraminiferal community resulting in a growth in biomass. The BFAR is therefore considered to be a reliable proxy for reconstructing export of organic matter and to the sea floor (van der Zwaan et al, 1999). This means that in most cases organic matter is the main limiting factor for the accumulation of benthic foraminifera. However, extreme environmental conditions (e.g. low-oxygen levels) lead to a decrease in the amount of benthic foraminifera (van der Zwaan et al, 1999). In that case oxygen becomes the limiting factor for the growth of the benthic foraminiferal community. This is the case for Mediterranean sapropels. During sapropel formation the diversity and abundance of benthic foraminifera decreases significantly (e.g. Jorissen, 1999; Morigi, 2009).

Furthermore, certain species thrive under (semi-)stressed environments resulting in high dominance (van der Zwaan et al, 1999). This is apparent in the TROX-model as well. It shows that only deep infaunal species exist in the anoxic zone. This is the case for Mediterranean sapropels where deep infaunal taxa are generally dominant (Schmiedl et al., 2003). During very extreme environments the whole benthic foraminiferal community can be removed. This is the case for some intervals within Mediterranean sapropels (Schmiedl et al., 2003; Morigi, 2009). In conclusion, sediment supply must be taken into account for BFAR reconstructions. A high sediment supply dilutes the amount of benthic foraminifera per gram. In contrast, low sediment supply results in a relative increase in benthic foraminifera per gram.

In the past, studies have used the abundance of certain specific species to interpret the paleodepth, salinity and water temperature. Figure 5 explains that caution must be exercised by those interpretations (van der Zwaan et al, 1999). It shows that the waterdepth range where species live depends greatly on the amount of organic flux. In most cases the organic flux regularly decreases with depth. However, the initial amount of incoming organic flux can vary greatly. This has a significant impact on the depth range of benthic foraminiferal species. In the modern Mediterranean Sea the distribution of the most dominant taxa of benthic foraminifera is controlled by the organic flux to the sea floor (de Rijk et al., 2000). Furthermore, there is a bathymetrical succession of species that is controlled by the amount of available organic matter. Therefore, individual species are not indicative of a certain water depth, but rather of a certain amount of organic flux.

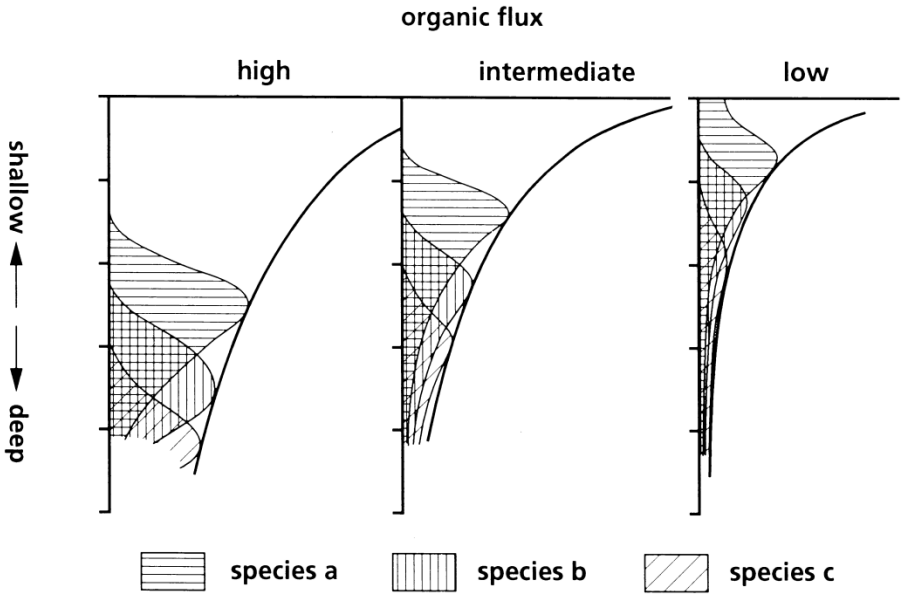

Fig. 5 – The high sensitivity of benthic species to organic flux. The depth range of species changes with the availability of organic matter. Therefore care must be taken with paleodepth reconstructions (van der Zwaan et al., 1999)

This figure and the TROX-model both show that benthic foraminifera are not stenotopic to factors as salinity, oxygen content or paleodepth. Waterdepth is not the only reason of the depth distribution of species, the ratio of organic matter and oxygen is in general more important (van der Zwaan et al, 1999; de Rijk et al., 2000).

Although benthic foraminifera are not stenotopic to salinity, they can still be indicative of salinity fluctuations (van der Zwaan, 1999). A differentiation can be made about the tolerance of species towards raised salinity levels. In this way salinity can be reconstructed roughly: hypersaline, brackish and normal marine environments can be distinguished (Murray 1991; van der Zwaan, 1982, van der Zwaan 1999). Nonetheless, there are better tools available today for salinity reconstructions.

During the MSC benthic foraminifera are largely absent in the Mediterranean due to high stress. If present, the benthic foraminifera are poorly diversified or even monospecific and consist of rare stress tolerating taxa (Rouchy and Caruso, 2006; Lozar et al., 2010; Pierre et al., 2011).

In open marine environments, the P/B ratio is considered to be most reliable for reconstructing the paleodepth (van der Zwaan et al, 1999; van Hinsbergen et al., 2005). Because the organic flux decreases with water depth, the amount of benthic foraminifera decreases with water depth as well. This is because benthic foraminifera live on the seafloor or within the seafloor sediments. This causes a relative increase in planktonic foraminifera. Therefore the percentage of planktonic foraminifera increases with depth (van der Zwaan et al., 1990). Van der Zwaan et al. (1990) developed a depth function based on the P/B ratio (%P) of living foraminifera of various sites:

$$\text{Depth} = e^{(3.58718 + (0.03534 \cdot \%P))}$$

However, the P/B ratio is sensitive to oxygen deficiency (van der Zwaan et al., 1999). Although the function corrects for small changes in oxygen levels, it is not applicable for strongly oxygen-deficient or anoxic environments (van der Zwaan et al., 1990).

3. Methods

This study makes use of the samples collected from the Ain el Beida section, which is located near Rabat, Morocco (Krijgsman et al., 2004). Of the 297 samples collected, 55 were selected for detailed benthic foraminiferal analyses. The samples were dry-weighed, disintegrated in water and washed over 63, 125 and 595 µm sieves at Utrecht University, Dept. of Geosciences. Splits of the 125 µm size fraction obtained with an Otto microsplitter were sent to the Department of Earth Sciences in Parma (Italy) for biostratigraphy (Krijgsman et al., 2004). The same sample set was previously used in the studies of Krijgsman et al. (2004) and van der Laan et al. (2005) for magnetostratigraphy, stable isotope analysis on the species *Planulina ariminensis* and for biostratigraphy on planktonic foraminifera and calcareous nannofossils.

The 55 samples selected for this study were chosen in parts of the stratigraphy that are characterized by the most distinct alternations of red marls and light beige marls. In these parts the red marls are more prominent (thicker and darker) and this means greater contrast with the light beige marls. The argument for this choice was that in this way it was more likely to find the astronomical signal in the benthic assemblages. The selected sedimentary cycles are AEB 27 to 29, AEB 32 to 34 and AEB 42 to 44 (Figure 3). The sedimentary cycles were studied in detail counting all available samples apart from AEB 42 to AEB 44. Cycles 27-29 and 32-34 were studied in high resolution with 7-8 samples per cycle. This is equivalent to approximately 3 samples per meter. Because the benthic foraminiferal assemblages were rather different, cycles 42-44 were studied in less detail with 4 samples per cycle. This is equivalent to approximately 1.5 samples per meter.

The washed residues were split with a microsplitter to obtain a minimum of 200 benthic foraminifera in every sample. The foraminifera were picked with a wet brush, mounted on micropaleontology slides, identified to species level and counted. The taxonomic concept of Holbourn et al. (2013) was used for identification of species and if this proved impossible, genera. The data-set was constructed from digitalization of the counts and identification of the foraminifera, and from the counts the relative frequencies, i.e. the percentage of species in the samples, were calculated.

The P/B ratio is expressed as %P=100*P/(P+B), where P is the number of planktonic foraminifera and B is the number of benthic foraminifera in a sample. This was determined for all samples during the process of splitting. The species diversity is expressed as Shannon index H (Spellerberg and Fedor, 2003) and is calculated as follows:

$$H = -\sum_{i=1}^{n} pi \ln pi$$

In this formula *i* is the index, *n* is the total number of species in a sample and *p* is the relative abundance of a species in a sample. The total amount of benthic foraminifera per gram was calculated for all samples using the dry weights and the split size.

The transfer function of Hohenegger (2005) is used for a comprehensive paleodepth reconstruction. The function is based on the maximum depth ranges of benthic foraminiferal taxa (see Pérez-Asensio et al. (2012) for overview and application). The paleodepth is calculated as follows (Pérez-Asensio et al., 2012):

$$\text{paleodepth (m)} = \sum \left(n_j l_j d_j^{-1} \right) / \sum \left(n_j d_j^{-1} \right)$$

In this formula n_j is the relative abundance of the jth species, l_j is the mean of the depth range of the jth species and d_j is the standard deviation of the depth range of the jth species. Table 1 displays the maximum depth range of the species used in this study (>2% in relative abundance in the data-set).

Species	Minimum depth	Maximum depth	Mean	Standard deviation
Bolivina dilatata	15	3000	1507.5	1492.5
Bulimina aculeata	5	5000	2002.5	1997.5
Bulimina striata	50	3241	1645.5	1595.5
Cibicides lobatus	20	750	385	365
Cibicidoides dutemplei	100	600	350	250
Cibicidoides pachyderma	30	4000	2015	1985
Cibicidoides ungerianus	50	4000	2025	1975
Globocassidulina subglobosa	50	4000	2025	1975
Gyroidina soldanii	100	5000	2550	2450
Melonis barleeanus	13	3974	1993.5	1980.5
Melonis soldanii	90	1000	545	455
Oridorsalis umbonatus	65	4000	2032.5	1967.5
Planulina ariminensis	70	1300	685	615
Pullenia bulloides	60	4000	2030	1970
Siphonina reticulata	55	1500	777.5	722.5
Trifarina bradyi	0	600	300	300
Uvigerina pigmea	100	4400	2250	2150

Table 1 - Depth ranges of benthic foraminiferal taxa used in this study with mean and standard deviation. The maximum depth ranges are obtained from van Hinsbergen et al. (2005) and mainly Pérez-Asensio et al. (2012); Table 1.

In order to explore patterns and cyclicity in the data-set the statistical package PAST 3.1 was used (Hammer et al., 2001). Single and rare occurrences were removed from the relative frequency data, and so were species occurring <2% in any sample. This was done to remove the noise and obtain a more robust data-set. Furthermore, specimens that could not be identified to species level were removed as well, as different species within a genus could indicate different environmental conditions. The PAST program was used for multivariate hierarchical cluster analysis and principal component analysis (PCA).

Hierarchical clustering is applied to gain more insight in the correlation between samples and species. Different types of clustering were performed on different parts of the section. The UPGMA method with 'correlation' as similarity index gave the most consistent and evident results. In this 'within group linkage' method a similarity matrix is constructed. The distance between two clusters is

defined as the average of the distance between all pairs of samples whereby one member of the pair is from each of the cluster. Principal component analysis is used to explore the significance and nature of possible factors responsible for the variance in the data-set. These results show patterns in the data-set and are used for reconstructing environmental changes.

4. Results

4.1 *Benthic foraminiferal assemblages*

A total of 74 different species and genera were recognized. An overview of the counts of benthic foraminifera in the samples of the Ain el Beida section can be found in Appendix1. Figure 6 shows that the distribution patterns of *Uvigerina pigmea*, *Bulimina striata, Cibicidoides pachyderma* and *Hanzawaia boueana* correlate with the different lithologies. This shows that precessional scale distribution patterns are clearly present. The figure shows that in most cases *U. pigmea* and *C. pachyderma* are more abundant in the red marls and less abundant in the light beige marls. The relative abundances of *H. boueana* and especially *B. striata* are in good agreement with the cyclic alternations of the marls. They are more abundant in light beige marls and less abundant in red marls. Deviations from this general pattern are present in sedimentary cycles 27 and 28 (Fig. 6).

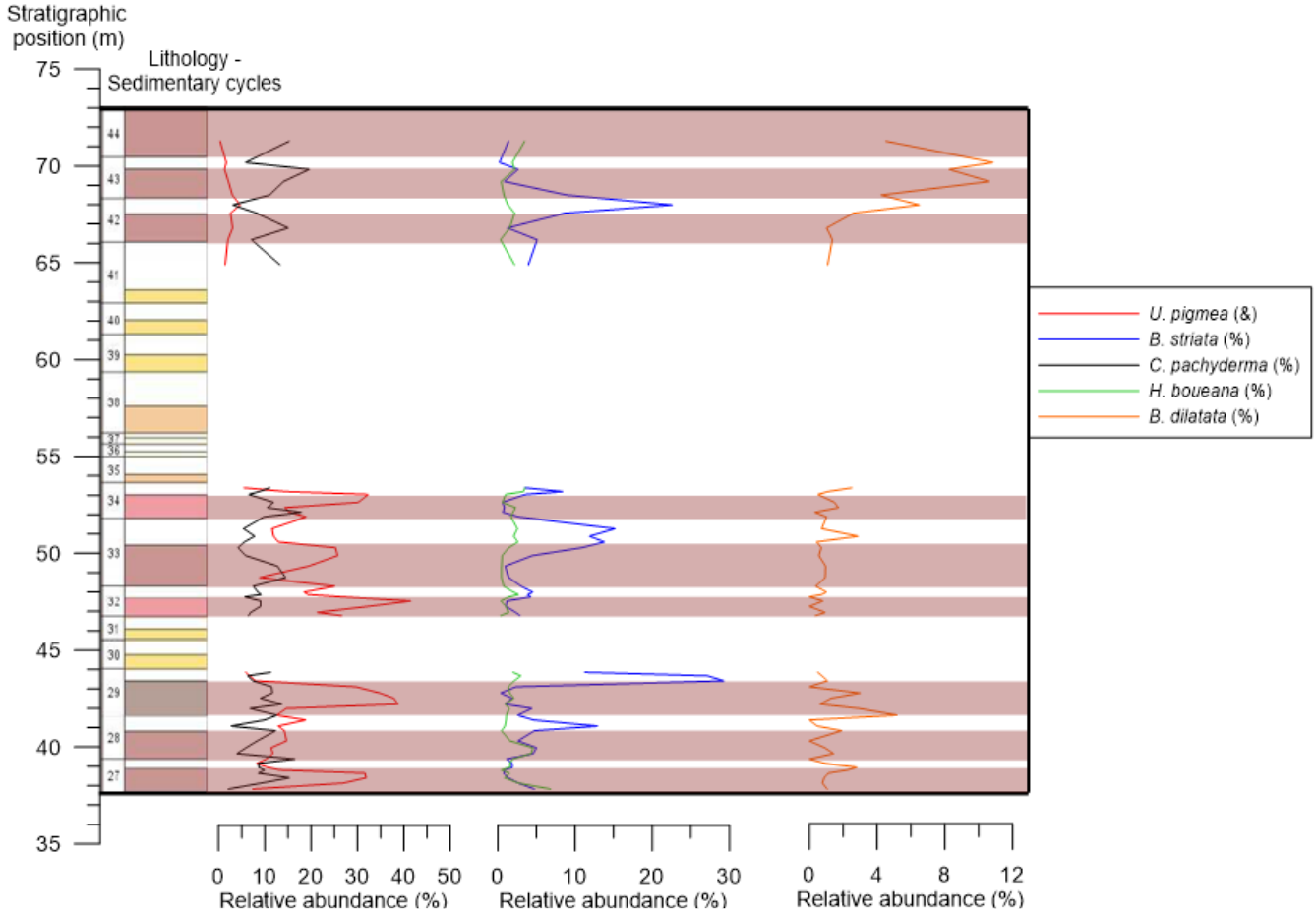

Fig. 6 – Relative abundances of *U. pigmea, C. pachyderma, B. striata, H. boueana* and *B. dilatata* (%) against depth (m) and lithology. For clarity the abundances are plotted on different X-axes

The amplitude of the relative abundances of the species varies, especially for *B. striata*. Furthermore, the relative abundances of *U. pigmea* and *B. striata* are relatively high compared to other species. In several samples they reach 30-40% relative abundance.

In Figure 6 it can be seen that the relative abundance of *U. pigmea* is on average four times lower in the upper part of the studied section (cycles 42 - 44). Other species show changes in depth

distribution as well. The relative abundance of *Bolivina dilatata* is 5 times higher in cycles 42 - 44 (Fig. 6). Furthermore, *Cibicidoides dutemplei* is more abundant and *Oridorsalis umbonatus* is less abundant in in cycles 42 - 44.

***4.2** P/B ratio, species diversity, bf/g*

Figure 7 shows the benthic foraminiferal counts per gram (bf/gram), the species diversity (Shannon index) and the P/B ratio (expressed as percentage planktonic foraminifera, %P) against lithology. Precessional scale variations are clearly present.

The P/B ratio shows a consistent pattern of high values in light beige marls and low values in red marls. The high amplitudes in cycles 42-44 are explained by the low sample resolution and by sampling in mainly the midpoints of the marls. Light beige marls generally have 70-90% planktonic foraminifera. Red marls generally have 50-70% planktonic foraminifera. The red marl of cycle 28 does not show a definite decline in %P. There are variations on a sub-precessional scale in the red marls of cycles 28, 29, 33 and 34. There is no long-term trend in the P/B ratio.

The assemblages are generally more diverse in the light beige marls and less diverse in the red marls. A deviation to this pattern is the relatively high diversity in the red marl of cycle 28. As with the P/B ratio, variations on a sub-precessional scale are present in the red marls of cycles 28, 29, 33 and 34.

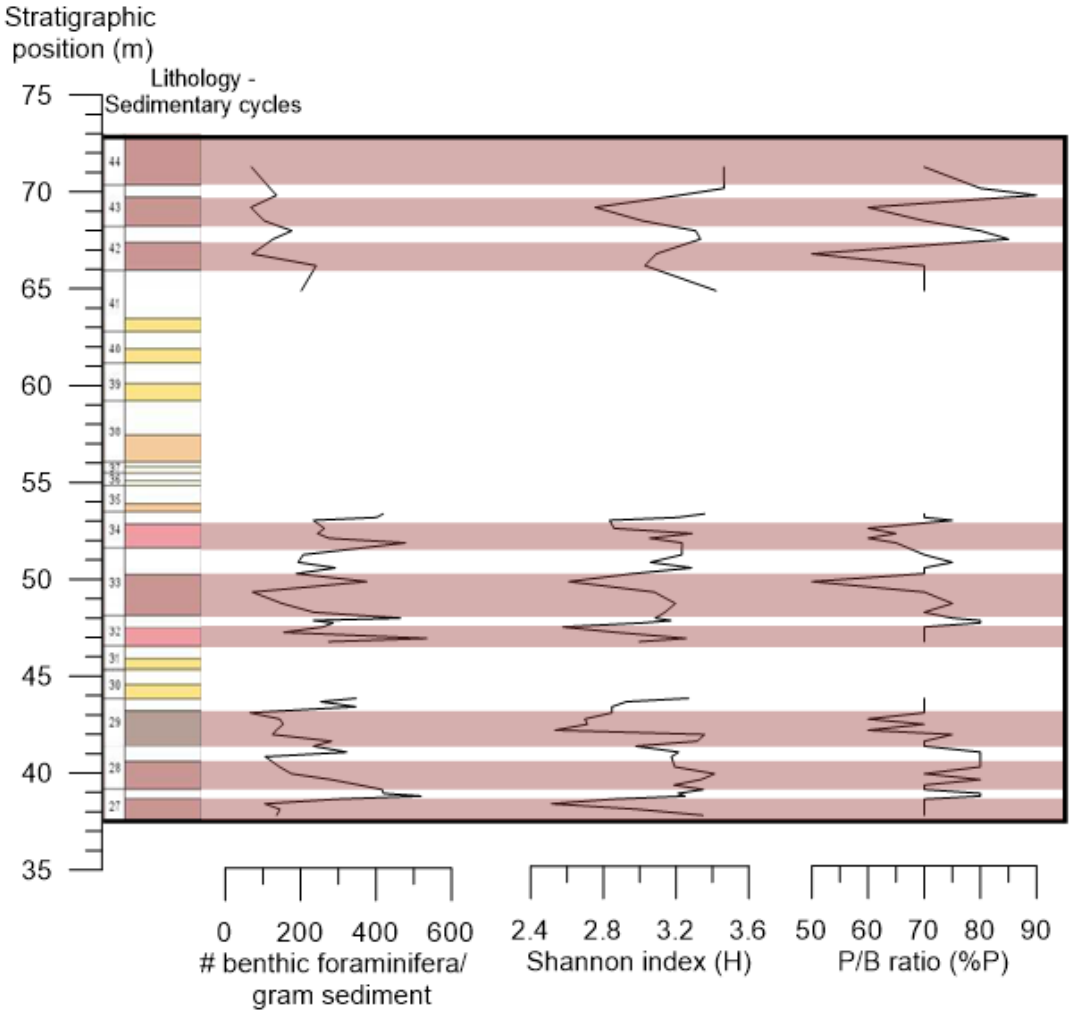

Fig. 7 – Benthic foraminiferal counts (bf/g), Species diversity (Shannon index) and P/B ratio (%P) against lithology

The benthic counts show that there are in general more benthic foraminifera per gram of sediment in the light beige marls and less in the red marls. Deviations to this pattern can be found in three peaks in the red marls of cycle 32, 33 and 34 and in a minimum in the light beige marl of cycle 33. Apart from the deviations there are in general there are 100-300 benthic foraminifera per gram of sediment in the red marls and 300-500 in the light beige marls. This is not the case for the cycles 42-44. Here, the amount of benthic foraminifera per gram sediment is significantly reduced in both the red and light beige marls. Variations on a sub-precessional scale are present in the red marls of cycles 29, 32, 33 and 34.

4.3 *Cluster analyses*

Figure 8 shows a dendrogram resulting from hierarchical clustering performed on all samples. From the figure it is clear that a group of samples from the red marls are very similar to each other. In cluster 1 the correlation of 14 red marl samples is above 0.9. This means that these samples are very similar in the distribution of benthic foraminifera. The samples from the light beige marls correlate less well. This is apparent from cluster 2, which contains 7 light beige marls samples with a correlation of 0.65 or above. Other beige marl samples correlate more with red marl samples. Cluster 3 shows that the samples from the upper part of the section, cycles 42 to 44, correlate more to each other than to other samples. However, the correlation is not very high. Furthermore, the analysis shows no distinction between beige marl samples and red marl samples of cycles 42-44. Figure 8 also shows that the analysis does not indicate a difference between bottom, mid or top samples from a lithological unit. These are present within the same cluster.

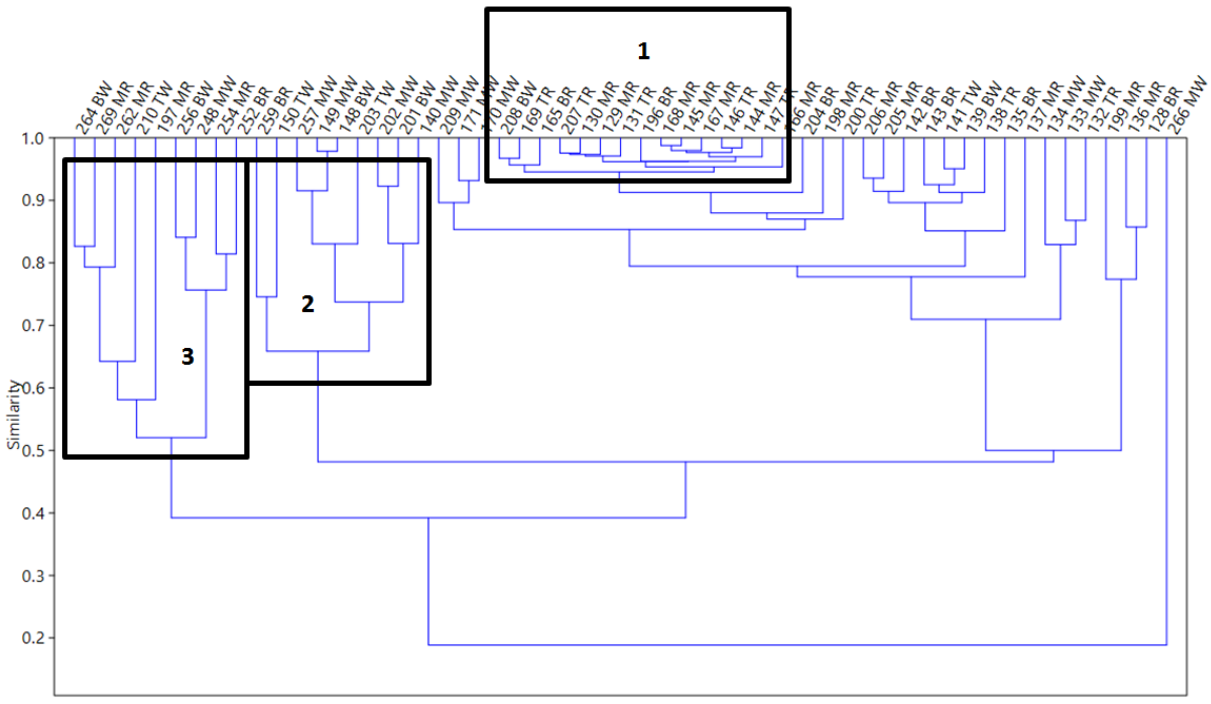

Fig. 8 – Dendrogram resulting from hierarchical clustering on all samples. Algorithm: Paired group (UPGMA). Similarity index= correlation. The samples on the x-axis are indicated with their sample number and lithology initials. These are: BR= bottom red MR= mid red TR= top red. BW= bottom white MW= mid white TW= top white. Red stands for red marls and white stands for light beige marls.

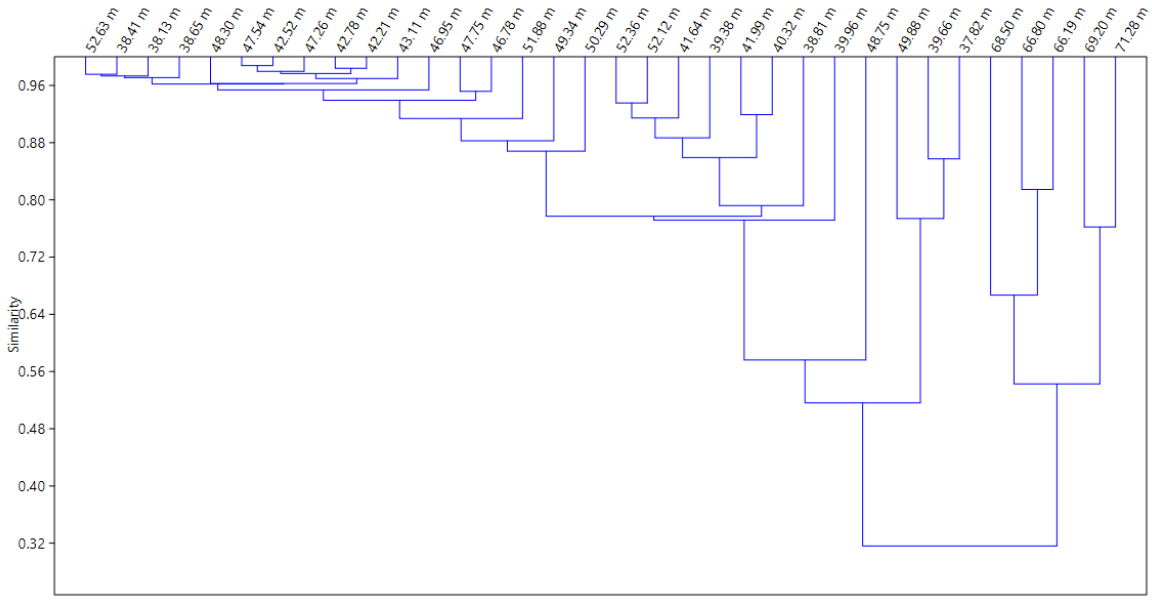

Fig. 9 – Dendrogram resulting from hierarchical clustering on all red marl samples. Algorithm: Paired group (UPGMA). Similarity index= correlation. The samples on the x-axis are indicated with their stratigraphy level in meters. In this way differences in depth are visible.

Figure 9 shows the result of hierarchical clustering on red marl samples. The left part of this dendrogram contains high-correlation samples which were present in cluster 1 from Figure 8 as well. They are from the middle and lower part of the section; cycles 27 to 29 and 32 to 34. The 5 samples in the cluster at the right side of the dendrogram correlate little with the other samples. These are from the upper part of the section; sedimentary cycles 42 to 44. From this figure and from Figure 8 it is clear that the middle and lower part of the section are more similar in species distribution and that the upper part is different.

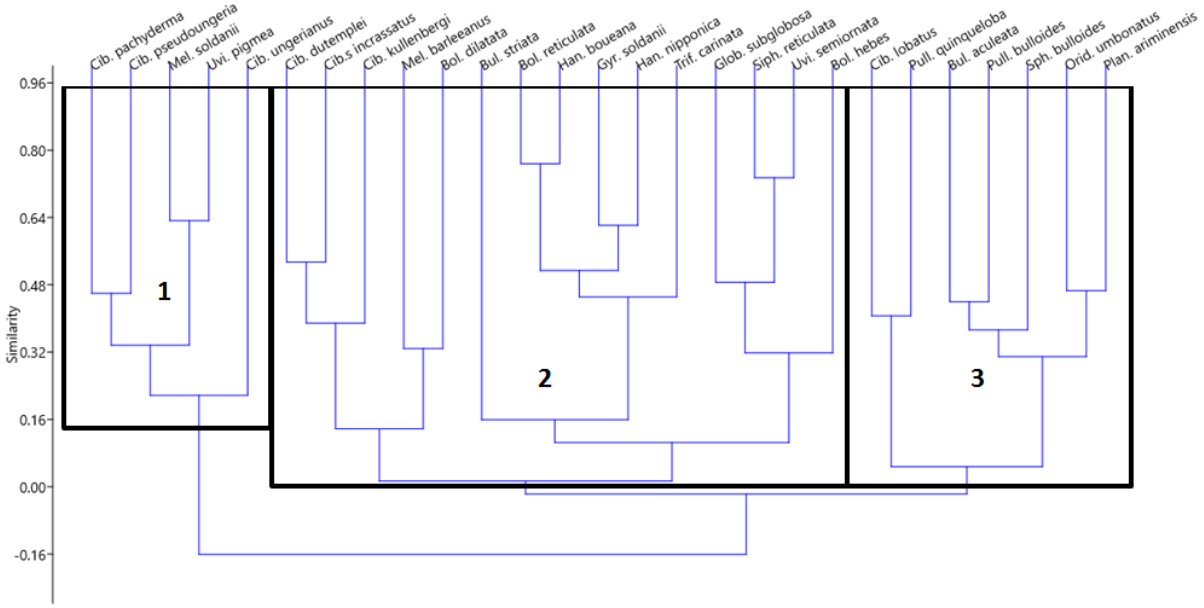

Fig. 10 – Result of hierarchical clustering on species of the samples of sedimentary cycles 27 to 29. Algorithm: Paired group (UPGMA). Similarity index= correlation. Cluster 1 contains species that are more abundant in red marls. Cluster 2 contains species that are more abundant in the light beige marls.

Figure 10 shows a dendrogram of hierarchical clustering of species on the lower part of the section; cycles 27 to 29. Cluster 1 shows species on the left side of the dendrogram that correlate relatively well. Cluster 2 and 3 shows the same for the species in the middle and at the right side of the dendrogram. The species of cluster 1 are generally more abundant in the red marls and the species of cluster 2 are generally more abundant in the light beige marls. Species of cluster 3 do not differentiate much between the red and light beige marls. The species of clusters 2 and 3 correlate negative to the species of cluster 1. The negative correlation means that the distribution patterns of cluster 2 and 3 are opposite to that of cluster 1.

4.4 *Principal component analysis*

The sample scores of the principal component analysis (PCA) are plotted against lithology in Figure 11. The first component (PC1) explains 52% of the variance of the data, which means that a significant part of the species distribution correlates to this variable. PC1 shows a pattern that is very similar to that of the relative abundance of *U. pigmea,* which is presented in Figure 6. PC1 has in general higher scores in red marls and lower in light beige marls. The pattern of PC2 is similar to that of the relative abundance of *B. striata* (Figure 6). The sample scores of PC2 are in general higher in the light beige marls and lower in the red marls. This diagram shows a match between the distribution of species and the cyclic alternations of red and light beige marls. Furthermore, PC1 shows a difference between the upper part of the section (cycles 42-44) and the two lower parts of the section (cycles 27-29 and 32-34).

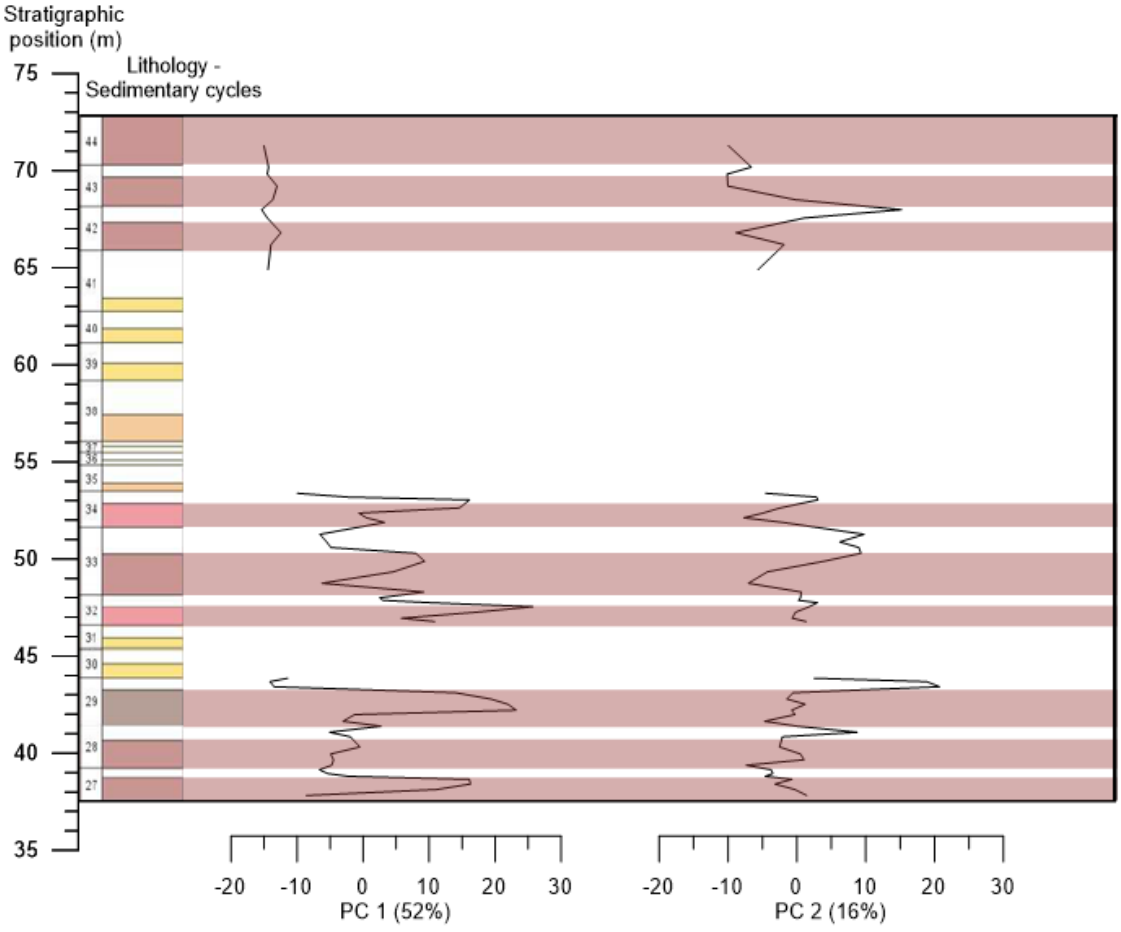

Fig. 11 – Result of principal component analysis on the reduced data-set against lithology. The eigenvalue of components 1 and 2 are 52% and 16% respectively.

Table 2 presents the species loadings on PC1 and PC2 of PCA on the samples of cycles 27 to 29 and 32 to 34, the middle and lower part of the section. Cycles 42-44 are not included because the upper part of the section has a rather different benthic foraminiferal distribution that disturbs the signal. The correlation value of *U. pigmea* is 0.98 for the first component. For component 2 the value of *B. striata* is 0.77. The four species that have the highest loadings for the first component are presented in red. These are present in cluster 1 of Figure 10 as well. The eleven species with the lowest loadings for the first component are presented in blue. Nine of these species are present in cluster 2 of Figure 10.

Species	PC 1 (53%)	PC 2 (16%)
Bolivina dilatata	-0.16022	-0.23886
Bolivina hebes	-0.14012	-0.11511
Bolivina reticulata	-0.17455	0.023395
Bulimina aculeata	-0.13828	-0.32026
Bulimina striata	**-0.60125**	**0.77332**
Cibicides lobatus	-0.05067	0.12335
Cibicidoides dutemplei	**-0.30093**	0.021239
Cibicidoides incrassatus	-0.04523	0.054313
Cibicidoides kullenbergi	**-0.2172**	-0.16693
Cibicidoides pachyderma	**0.2253**	-0.56651
Cibicidoides pseudoungerianus	**0.1532**	-0.09998
Cibicidoides ungerianus	0.032106	-0.25598
Globocassidulina subglobosa	**-0.24943**	-0.12981
Gyroidina soldanii	**-0.6017**	-0.16813
Hanzawaia boueana	**-0.46121**	0.063213
Hanzawaia nipponica	**-0.51393**	-0.04194
Melonis barleeanus	-0.14167	-0.2377
Melonis soldanii	**0.1802**	-0.20522
Oridorsalis umbonatus	**-0.33155**	0.031759
Planulina ariminensis	**-0.31029**	-0.09286
Pullenia bulloides	0.054665	-0.18395
Pullenia quinqueloba	0.049397	-0.16491
Siphonina reticulata	-0.25427	-0.2477
Sphaeroidina bulloides	0.095702	-0.2543
Trifarina carinata	**-0.42798**	-0.18858
Uvigerina pigmea	**0.97965**	0.19847
Uvigerina semiornata	**-0.33318**	-0.2069

Table 2 – Correlation values of the loadings of the benthic foraminifera in the samples of sedimentary cycles 27 to 29 and 32 to 34

The results of Figures 6 and 10 confirm that species indicated in red in table 2 have similar distribution patterns throughout the section. The same applies for the species indicated in blue. In addition, these results indicate that the distribution patterns of red and blue species throughout the section are opposite to each other.

In Figure 12 the relative abundances of the species indicated in red are added up in group 1a. The relative abundances of the species indicated in blue are added up in group 2a. The figure clearly shows the relation between the two groups and lithology. Group 1a has higher values in the red marls and lower in the light beige marls. The opposite is the case for group 2a. Because *U. pigmea* and *B. striata* have a high dominance in many of the samples they reduce the signal of the other

species significantly. This is known as the 'closed sum effect' whereby the high frequencies of the dominant species suppress the frequencies of other species. To see whether the suppressed species show the same signal, groups b and c are constructed.

Group 1b contains the sum of the relative abundances of the species indicated in red in Table 2, but the relative abundance of *U. pigmea* is divided by four. Group 2c contains the sum of the relative abundances of the species indicated in blue in Table 2, but the relative abundance of *B. striata* is divided by 2. Group 1c contains the sum of the relative abundances of the species indicated in red in Table 2, but without U. *pigmea*. Group 2c contains the sum of the relative abundances of the species indicated in blue in Table 2, but without *B. striata*. In this way it can be seen if the other species in the groups show the same signal.

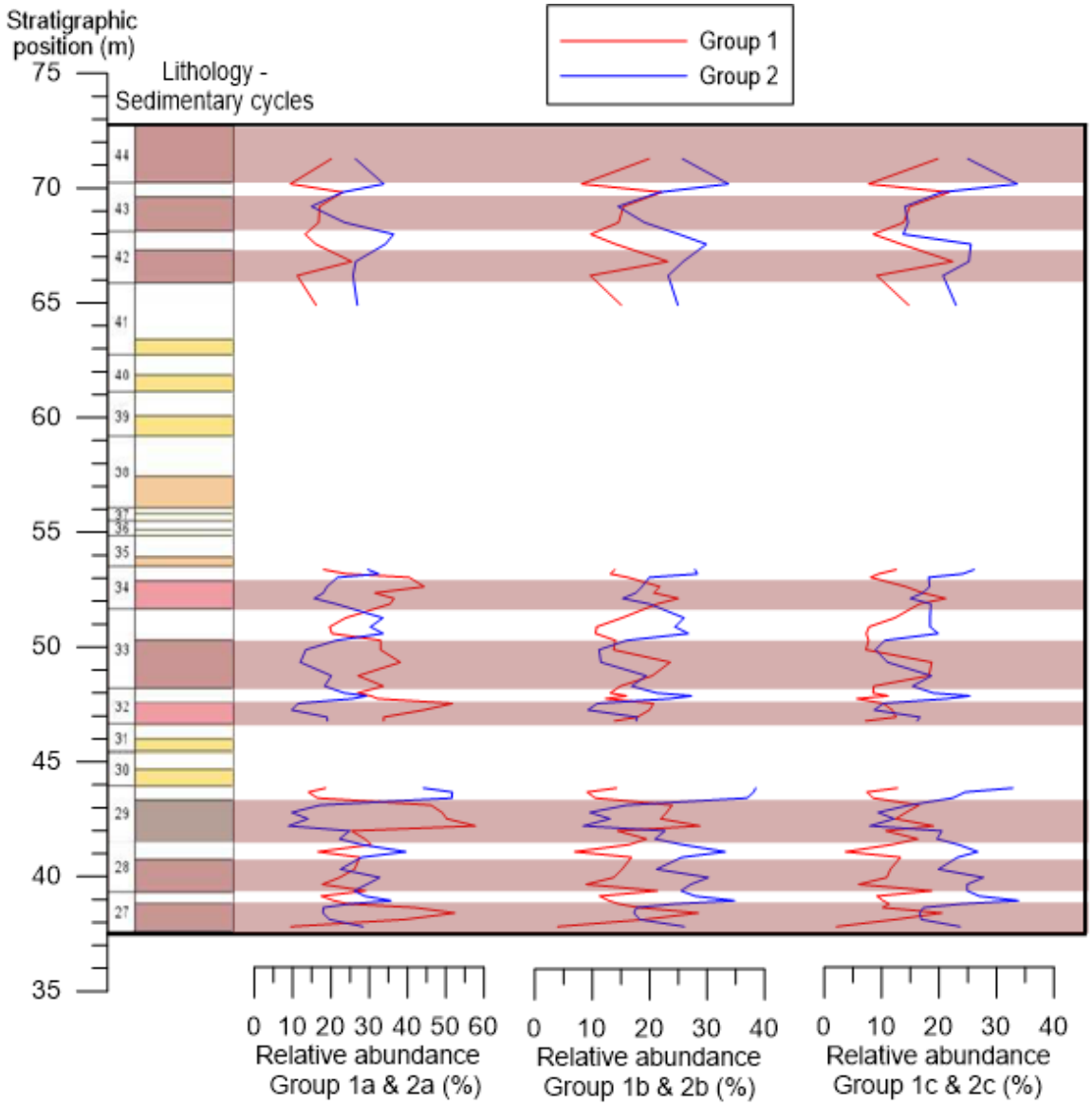

Fig. 12 – Groups 1 and 2 in relative abundances (%) against lithology. Groups a= original abundances. Groups b= abundances of *U. pigmea* and *B. striata* divided by 4 and 2 respectively. Groups c= abundances of *U. pigmea* and *B. striata* removed.

For all the different types of groups the relationship with lithology is still very clear. This means that without *U. pigmea* and *B. striata* the signal is still present. This is an important result because it means that the distribution of several benthic foraminiferal species matches with the precessional scale cyclic alternations of red and light beige marls. These are *B. striata, C. dutemplei,*

C. kullenbergi, C. pachyderma, C. pseudoungerianus, Globocassidulina subglobosa, Gyroidina soldanii, H. boueana, H. nipponica, Melonis soldanii, O. umbonatus, P. ariminensis, Trifarina carinata, U. pigmea and *U. semiornata.* There are sub-precessional scale variations as well. These are the minima of group 1 and the maxima of group 2 in the red marls of cycle 28 and 29. These variations are present in Figure 7 as well.

4.5 *Comparison with other records of the Ain el Beida section*

Figure 13 demonstrates that the pattern of the relative abundances of Groups 1 and 2 from this study is very similar to the patterns of the colour reflectance , PC-1 ICP (principal component 1 of the chemical composition) and the benthic and planktonic $\delta^{18}O$ record of the Ain el Beida section. Maxima in PC-1 are associated with increased fine-grained clastic material relative to carbonate (van der Laan et al., 2012). All the records show a strong relation between amplitude variation and lithology. The strongest amplitudes of Groups 1 and 2 are found in the red marl of cycle 29, while a clear response in the red marl of cycle 28 is absent. The colour reflectance, the PC-1 and the benthic $\delta^{18}O$ record display a strong amplitude in the red marl of cycle 29 as well. Additionally, these records show a weaker amplitude in the red marl of cycle 28. Variations on a sub-precessional scale are recorded by the colour reflectance and PC-1 of the chemical composition in the red marls of cycles 28 and 29.

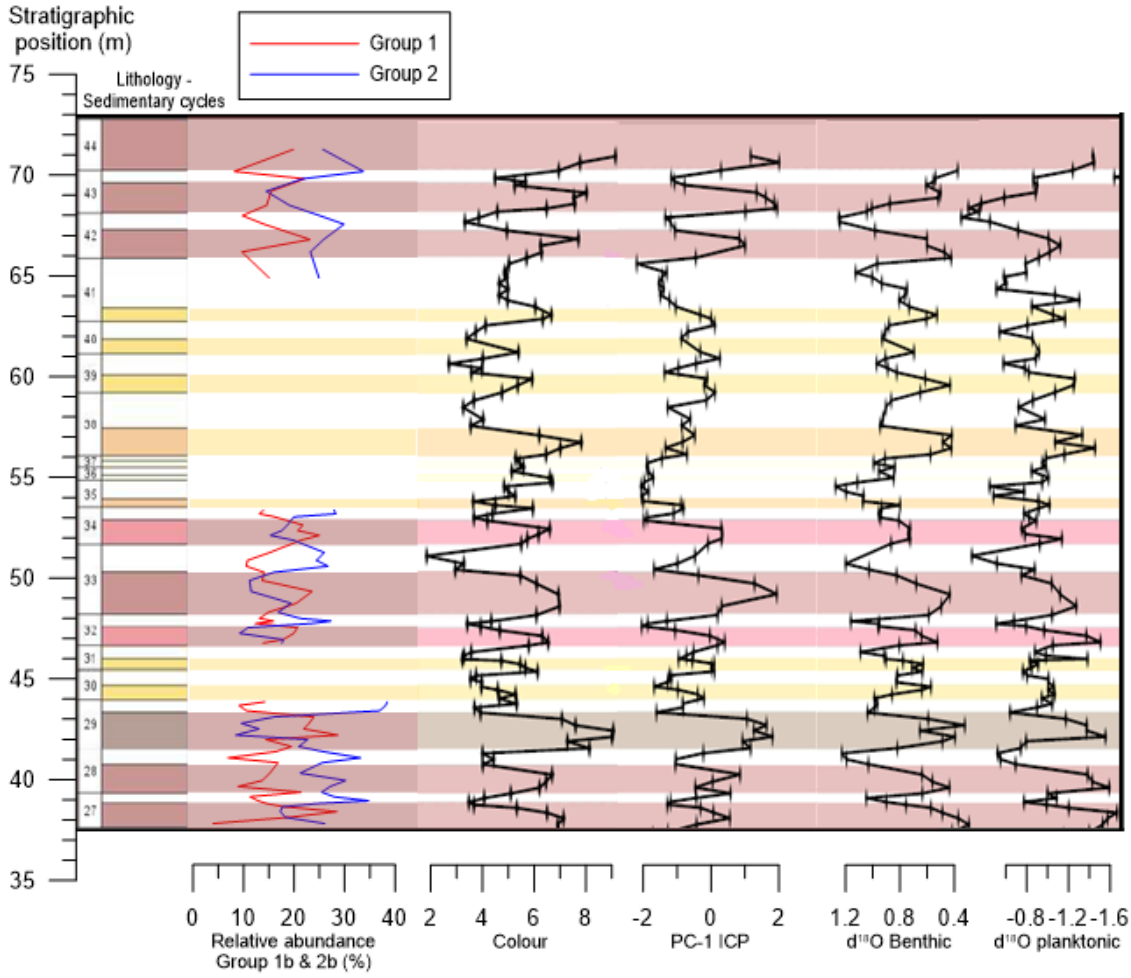

Fig. 13 – Groups 1 and 2 in relative abundances (%), colour reflectance, PC-1 ICP and the benthic and planktonic δ18O record against lithology. The colour reflectance, PC-1 ICP and the benthic and planktonic δ18O record are obtained from van der Laan et al. (2012).

5. Discussion

5.1 *Bathymetry*

A bathymetric reconstructing based on the benthic foraminiferal assemblages is performed to investigate if there are certain trends in paleodepth during the deposition of the Ain el Beida section. The depth function of van der Zwaan et al. (1990) based on the P/B ratio suggests precessional scale fluctuations in sea level between 200 and 900 m (Fig. 14 - Paleodepth A). However, the use of the P/B ratio in bathymetry is only applicable in an open marine environment (van der Zwaan et al, 1999; van Hinsbergen et al., 2005). The Ain el Beida section is located in the Rif Corridor. During the depositional phase there was probably much variation in fluvial run-off and possibly Mediterranean water mass fluxes (van der Laan et al., 2012). Therefore, it is not considered to be an open marine environment. In addition, precessional scale variations strongly dominate the P/B ratio (Fig. 7), indicating astronomically induced climate variations related to bottom water ventilation rather than paleodepth fluctuations (van Hinsbergen et al., 2005). This makes the P/B ratio not reliable for paleodepth reconstruction of the Ain el Beida section. Therefore, the benthic foraminiferal assemblages are used for an indication for paleodepth as well. Because the distribution of benthic foraminifera is generally the result of the availability of nutrients and oxygen, these bathymetric reconstructions must be interpreted with care (van der Zwaan et al., 1999). However, by using a combination of several species, the paleodepth reconstructions are considered to be reliable.

There are many species in the assemblages that occur throughout the whole section. Many of these species are eurybathymetric, which means that the associated depth range is very wide (Murray, 1991; Perez-Asensio et al., 2012). Normally, stenobathymetric species live within a short range of waterdepth. There are no significant amounts (>2% of relative abundance) of known stenobathymetric species that indicate deep marine (>1000 m) environments, such as *Cibicidoides mundulus* and *Eponides spp.*, or upper shelf (<100 m) environments, such as *Ammonia spp.*, *Elphidium spp.* and *Valvulineria spp.* The combined abundances of *B. striata, C. dutemplei*, *C. lobatulus*, *C. pseudoungerianus, C. kullenbergi, Globocassidulina subglobosa, G. soldanii, P. ariminensis, Pullenia bulloides, Siphonina reticulata* and *Sphaeroidina Bulloides* in the samples suggest a waterdepth of 400-1000 m (Morkhoven et al., 1986; Berggren and Miller, 1989; van der Poel et al., 1992; van Hinsbergen et al., 2005).

The species *B. dilatata* and *C. dutemplei* are significantly more abundant in the youngest part of the studied section (Fig. 14). *C. dutemplei* is considered (near-) shelf taxa and normally lives at approximately 200-600 m waterdepth (Morkhoven et al., 1986; Berggren and Miller, 1989, van de Poel et al., 1992; De Stigter et al., 1998; Pérez-Asensio et al., 2012). *B. dilatata* can be present over a wide depth range (Pérez-Asensio et al., 2012). However, relatively high abundances of *B. dilatata* have been associated to (near)-shelf environments (De Stigter et al., 1998).

The transfer function of Hohenegger (2005) based on the depth ranges of various benthic foraminiferal taxa is used for a comprehensive bathymetric reconstruction. This reconstruction gives an estimation of paleodepth based on the maximum depth ranges of marker species. Table 1 displays the depth ranges of the 17 benthic foraminiferal species used in this study. To avoid local differences in depth distribution of benthic species, the maximum depth range described in literature is used. A consequence of this strategy is that the reconstructed paleodepth has a high uncertainty. Furthermore, the depth ranges are mostly based on living taxa and are assumed constant through time (Pérez-Asensio et al., 2012).

Figure 14 (Paleodepth - B) demonstrates the reconstructed paleodepth. As with the paleodepth reconstruction based on the P/B ratio, this reconstruction shows precessional-scale variations, suggesting an increase of 200-400 m in sea-level during red marl formation. This is not likely since glacio-eustatic sea-level fluctuations are obliquity controlled (Krijgsman et al., 1999b) and precessional-scale fluctuations in tectonic activity are excluded. These fluctuations are probably the result of variations in stress. The TROX-model (Fig. 4, Jorissen et al., 1995) shows that because of low-oxygen content only deep infaunal species exist in the anoxic zone. This is the case for Mediterranean sapropels where deep infaunal taxa are generally dominant (Schmiedl et al., 2003). A

similar process is observed in the red marls (associated with increased stress; lowered oxygen content and increased organic flux, discussed in **5.3.1**) where the relatively deep-water indicating species are more abundant.

Nevertheless, there are differences in the average paleodepth between the three studied intervals (Fig. 14). The average paleodepth during the older part of the section (5.95-5.88 Ma) is estimated between 900-1000 m. The middle part of the section (5.83-5.77 Ma) displays an average paleodepth of 1000-1100 m, while the younger part of the section (5.59-5.52 Ma) is estimated between 700-800 m. The difference between the oldest part and the middle part suggests an increase in paleodepth of approximately 50-150 m. Furthermore, *B. dilatata* and *C. dutemplei* show in average slightly higher abundances in the oldest part compared to the middle part (Fig. 14). However, these differences are not very substantial.

The difference in reconstructed paleodepth between the middle part and the younger part is significantly larger; approximately 200-300 m. Furthermore, the abundances of *B. dilatata* and *C. dutemplei* are five times higher in the younger part of the section (Fig. 14). These are strong indications for a decline in paleodepth in the Gharb basin towards the younger part of the section.

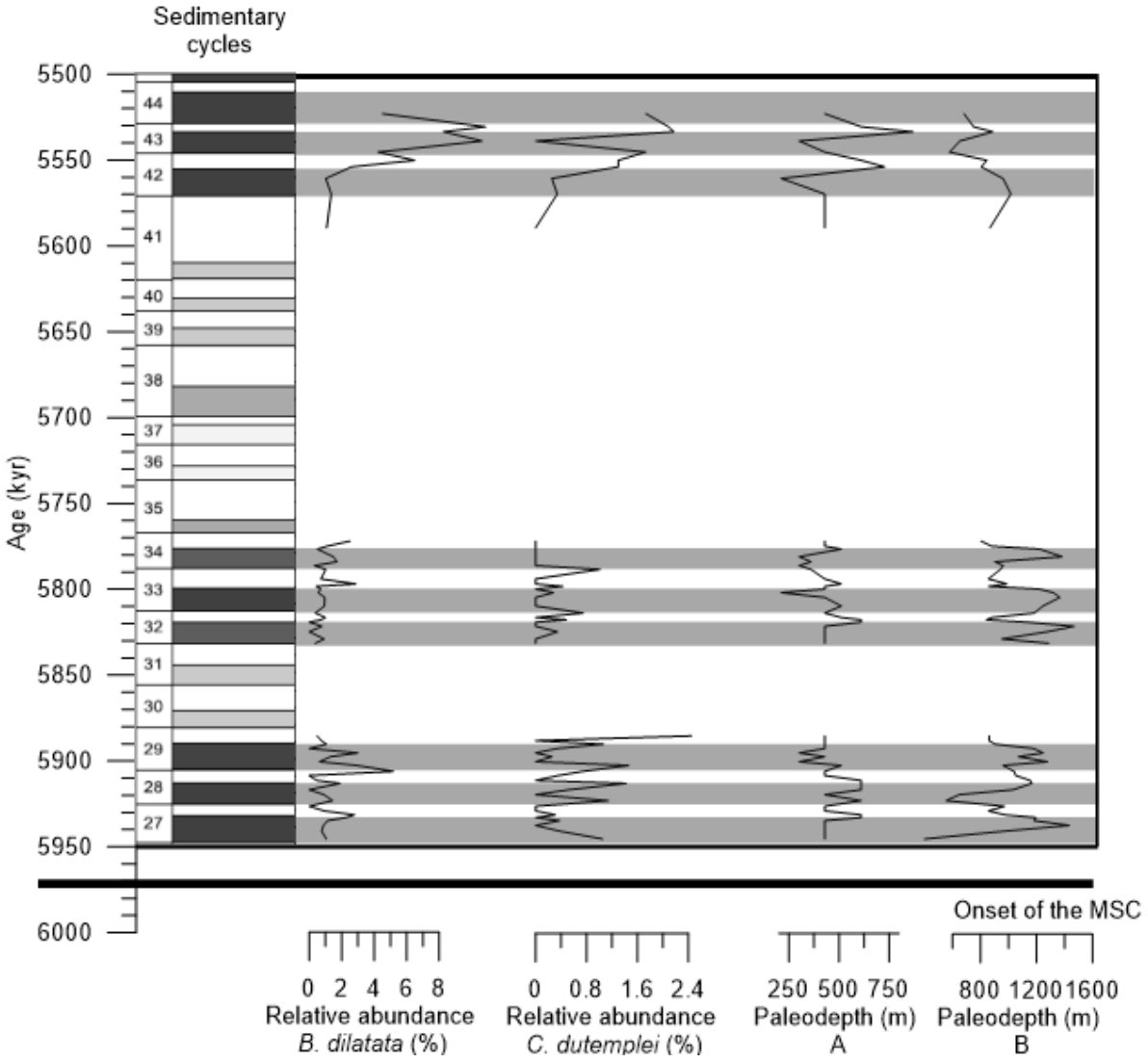

Fig. 14 – The relative abundances of *B. dilatata* and *C. dutemplei* (%) and the reconstructed paleodepth A and B plotted against age (kyr). A line that marks the onset of the MSC (5.97 Ma) is included as well. Paleodepth A is based on the depth function of van der Zwaan et al. (1990). Paleodepth B is based on the transfer function of Hohenegger (2005).

These results indicate that the paleodepth of the Gharb basin did not change significantly between 5.95-5.88 Ma and 5.83-5.77 Ma The paleodepth decreased between 5.77-5.52 Ma with an estimated depth of approximately 200-300 m. The decline of waterdepth continued within the younger part of the section. Evidence for this can be found in and the declining trend in the paleodepth reconstruction and the rising trend in relative abundance of *B. dilatata* and *C. dutemplei* towards sedimentary cycle 44 (Fig. 14).

The lowering in sea-level of the Gharb basin in the upper Miocene is consistent with the findings of Barbieri and Ori (2000). They analysed benthic assemblages of various other sections in the Gharb basin. They estimated a shallowing of the basin towards the Miocene-Pliocene boundary (5.33 Ma) of 300 m. Furthermore, the elemental composition of the Ain El Beida section indicates an increase in grainsize towards the younger part of the section (van der Laan et al., 2012). In addition, the calculated sedimentation rate of van der Laan et al., (2005) increases towards sedimentary cycle 44 (Fig. 16). This indicates a closer distance to the river mouth and supports the notion of a shallowing trend in the Gharb basin towards the end of the Miocene. The sea-level decline can be the result of glacio-eustatic or tectonic causes. However, the $\delta^{18}O$ record of the Ain El Beida and the Sale section (located near Ain El Beida) cannot validate a glacio-eustatic cause (Barbieri et al., 2000; van der Laan et al., 2005). Therefore, tectonic uplift is the most sensible explanation. The uplift can be considered as an extension of the tectonic explanation for the closing of the Rifian Corridor and the initiation of the MSC (Hodell et al., 2001; Krijgsman et al., 2004).

The onset of the Messinian Salinity Crisis (MSC) is indicated in Figure 14. It occurred before the deposition of the studied part of the section. This bathymetric reconstruction shows that despite the tectonic activity between Africa and Iberia that resulted in the isolation of the Mediterranean Sea, no tectonic uplift occurred in the Atlantic side of the Rifian Corridor during the first stage of the MSC. This probably allowed exchange between Mediterranean and Atlantic waters . The age interval of the sea-level lowering in the younger part of the section coincides with the second stage of the MSC (5.60-5.55 Ma). The extreme conditions during the second stage have been linked in literature to sea-level lowering and subsequently complete isolation (Krijgsman et al., 1999b; Hilgen et al., 2007; Manzi et al., 2013). The bathymetric reconstruction based on benthic foraminifera supports this notion.

5.2 *Astronomical signal*

The astronomical signal is clearly present in the benthic foraminiferal assemblages of the Ain el Beida section. The relationship between the precession index and Groups 1 and 2 is very strong. Precession minima coincide with maxima in Group 1 of the benthic foraminifera, and minima in Group 2. In Figure 15 the summed relative abundances of the benthic species of Groups 1 and 2 are plotted against age, the precession index, the obliquity parameter and the summer insolation curve at 65°N. Eccentricity (~100 kyr and ~400 kyr cycles) act as amplitude modulators for precession; this is visualized by the line connecting the maxima of the precession index.

Besides precession and eccentricity, the summer insolation curve is modulated by the obliquity parameter. However, at 65°N the influence of obliquity on the summer insolation is considered minor compared to precession (Laskar et al., 1993). For the studied intervals, the summer insolation curve is therefore similar to the precession index. Maxima in the 100 kyr and 400 kyr eccentricity cycle cause high amplitude variation in precession and summer insolation during, resulting in strongly expressed red marls during the studied interval (cycles 27-29, 32-34 and 42-44).

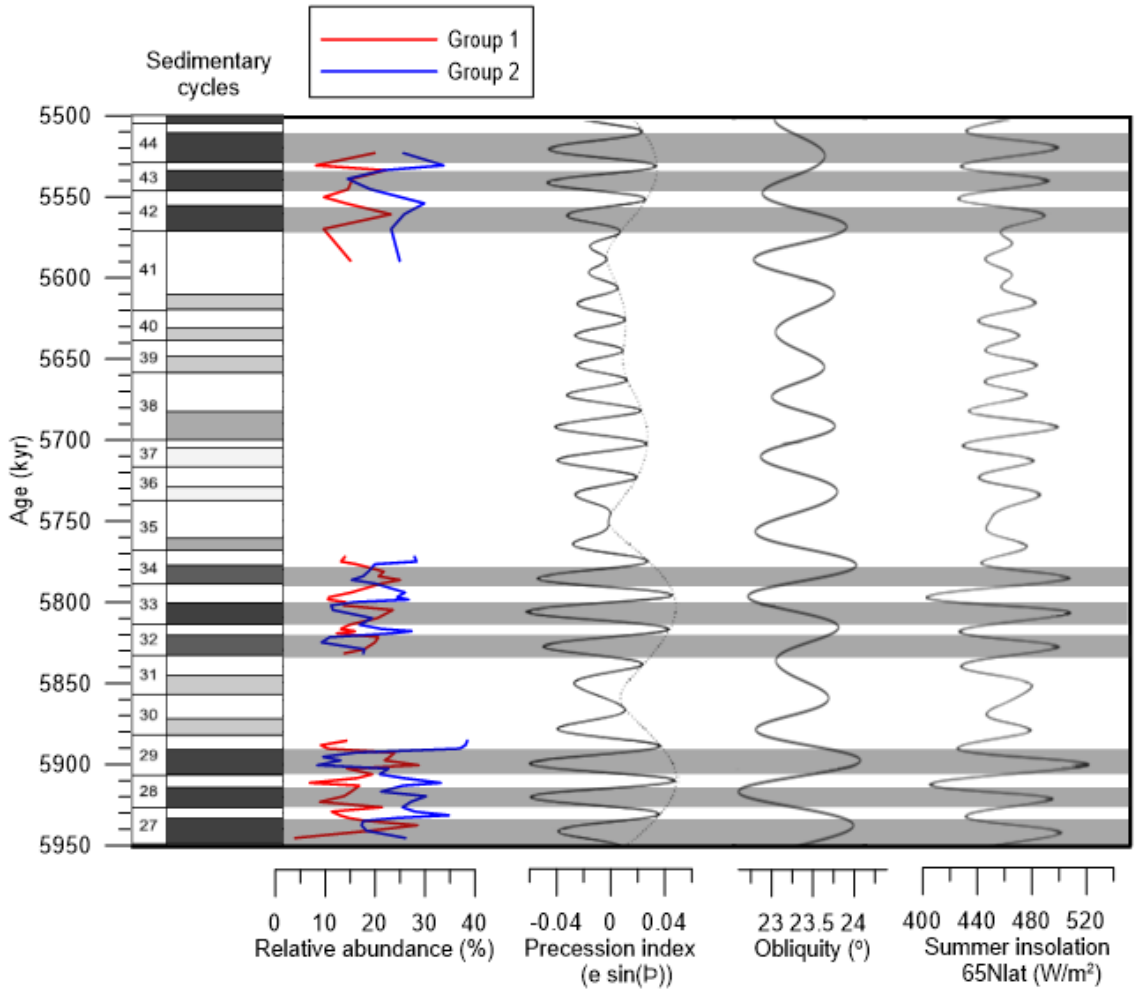

Fig. 15 – Relative abundances of Groups 1 and 2 compared to the precession index, the obliquity parameter and summer insolation at 65° N from the solution of Laskar et al. (1993). The studied red marls are indicated in black.

Interestingly, the obliquity parameter creates a reduction in the maximum of summer insolation in cycle 28 (Fig. 15). This is probably the reason for the absence of a clear response of Groups 1 and 2 to the astronomical forcing in the red marl of cycle 28. In contrast, the strongest maximum in summer insolation in this sequence at cycle 29 is linked to the strongest amplitudes of Groups 1 and 2. The obliquity parameter contributes here to the strong maximum in summer insolation and is probably causing the strong abundance amplitudes of Groups 1 and 2 at cycle 29. Figure 13 shows that the colour reflectance, PC-1 of the chemical composition (maxima associated with increased fine-grained clastic material relative to carbonate) and the benthic $\delta^{18}O$ record of the Ain el Beida section presented in van der Laan et al. (2012) also clearly show the same patterns in cycles 28 and 29. Consequently, the distribution of the benthic assemblages is mainly related to precession, modulated by eccentricity and with minor influence of obliquity.

The benthic and planktonic $\delta^{18}O$ values of the Ain el Beida section are controlled by precession, but show an obliquity signal as well (van der Laan et al., 2005). This also applies for the colour reflectance and chemical composition of the section (van der Laan et al., 2012). Figure 13 clearly shows that the astronomical signal in these proxies is in agreement with the signal in the benthic foraminiferal assemblages.

The astronomical signal is clearly present not only in the benthic foraminiferal assemblages, but also in the P/B ratio, species diversity (Shannon index) and the benthic foraminiferal counts per gram (Fig. 16).

Distortion of the astronomical signal

The pattern of the benthic counts in Figure 16 suggests that during the formation of red marls the amount of benthic foraminifera in the bottom waters is significantly decreased. However, here the process of distortion must be taken into account. Distortion occurs when there is a difference in sedimentation rate during the formation of the different lithological units. In the Ain el Beida section, the variations in sedimentation rate are positively correlated with precession amplitude (van der Laan et al., 2005). This results in the expression of thicker red marls and relatively thinner light beige marls. Therefore, signals (e.g. foraminifera per gram) in the red marls can be diluted. The calculated sedimentation rates of van der Laan et al. (2005) based on the astronomical tuning are presented in Figure 16. The effect of dilution is the strongest in the thickest, most expressed red marls such as AEB 33 (Fig. 16). In the lesser expressed red marls (e.g. AEB 39 t/m 41) the dilution effect is minor. This results in differences in thickness between the red marls; the red marl of AEB 33 is approximately four times thicker than the red marl of AEB 41 (Fig. 16).

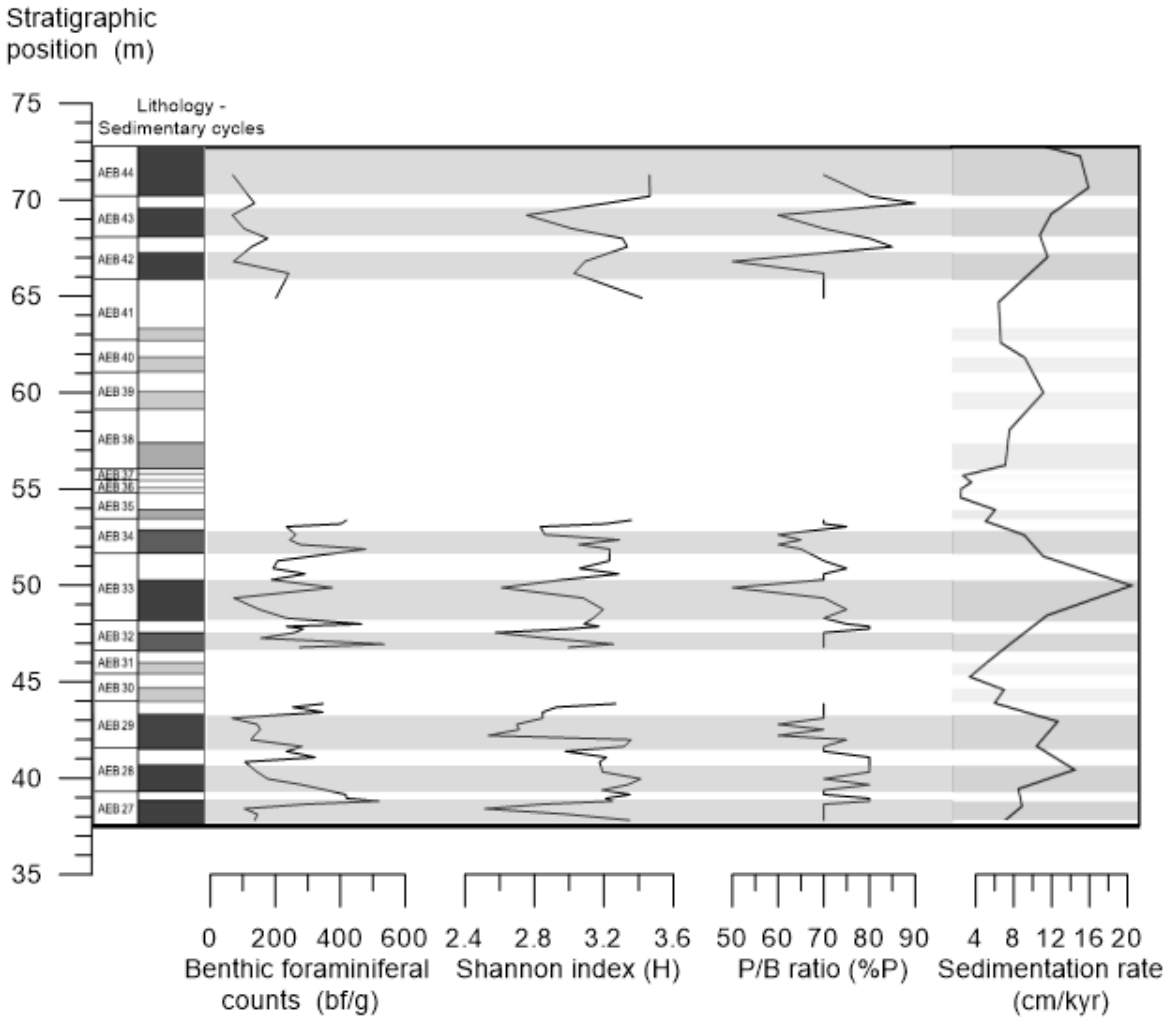

Fig. 16 – The benthic foraminiferal counts per gram, Shannon index, P/B ratio and sedimentation rate curve (see van der Laan et al. (2005) for details) against lithology.

The high sedimentation rate creates a distortion effect that reduces the benthic counts per gram in the red marls throughout the studied part of the section. Thicker red marls are more diluted resulting in stronger minima in the benthic counts of AEB 29 and AEB 33 (Fig. 16). Since the sedimentation rate curve of van der Laan et al. (2012) is based on the astronomical tuning, it has a

very low resolution. Therefore it is difficult to estimate the magnitude of dilution. Figure 16 demonstrates that the benthic counts are in general 2-4 times higher in the light beige marls. According to the modelled sedimentation rate of the Ain el Beida section form van der Laan et al. (2005) these differences may be fully explained by the effect of distortion.

The benthic foraminiferal counts display 100-300 benthic foraminifera per gram of sediment in the red marls and 300-500 in the light beige marls (Figs. 7, 16). The planktonic foraminiferal counts of the Ain el Beida section from van der Laan et al. (2012) show in general 50-200 planktonic foraminifera per gram of sediment in the red marls and 1000-1500 in the light beige marls. This transition is more extreme than the benthic counts. The reduction of planktonic foraminifera in the red marls is higher than the reduction of benthic foraminifera. This relative increase of benthic foraminifera in the red marls is reflected in the P/B ratio, which is lower in the red marls (Figs. 7, 16). However, the magnitude of the dilution effect is expected to be equal for benthic and planktonic foraminifera. Therefore, the relative increase of benthic foraminifera in the red marls can only be explained by changes in environmental conditions between the surface and bottom waters.

5.3 *Environmental conditions during the formation of the red and light beige marls*

The composition of the benthic foraminifera changes substantially between the light beige and red marls, as a result of changes in the environment. This is shown by the differentiation of the benthic species in group 1 and group 2 (Fig.13). The lowered species diversity observed in red marls is associated with an increase in stress (Murray, 1991; van der Zwaan et al., 1999).

5.3.1 Organic matter and oxygen

Figure 17 shows that the species *U. pigmea* is very dominant in de red marls. It reaches up to 30-40% in relative abundance. This is reflected by the Shannon index as well. Figure 17 demonstrates that maxima in relative abundance of *U. pigmea* correlate directly to minima in species diversity. These extreme amplitudes in relative abundances are best explained by intervals of upwelling. Upwelling is a common process along the shores of Northwest Africa (Altenbach et al., 1999; Guichard et al, 1999; Wang et al., 2015). The process of upwelling transports old organic matter from deeper parts of the ocean to the benthic ecosystem through lateral advection (Guichard et al, 1999). In addition, it transports nutrients to the primary producers in the surface waters resulting in an increase in organic flux to the bottom waters.

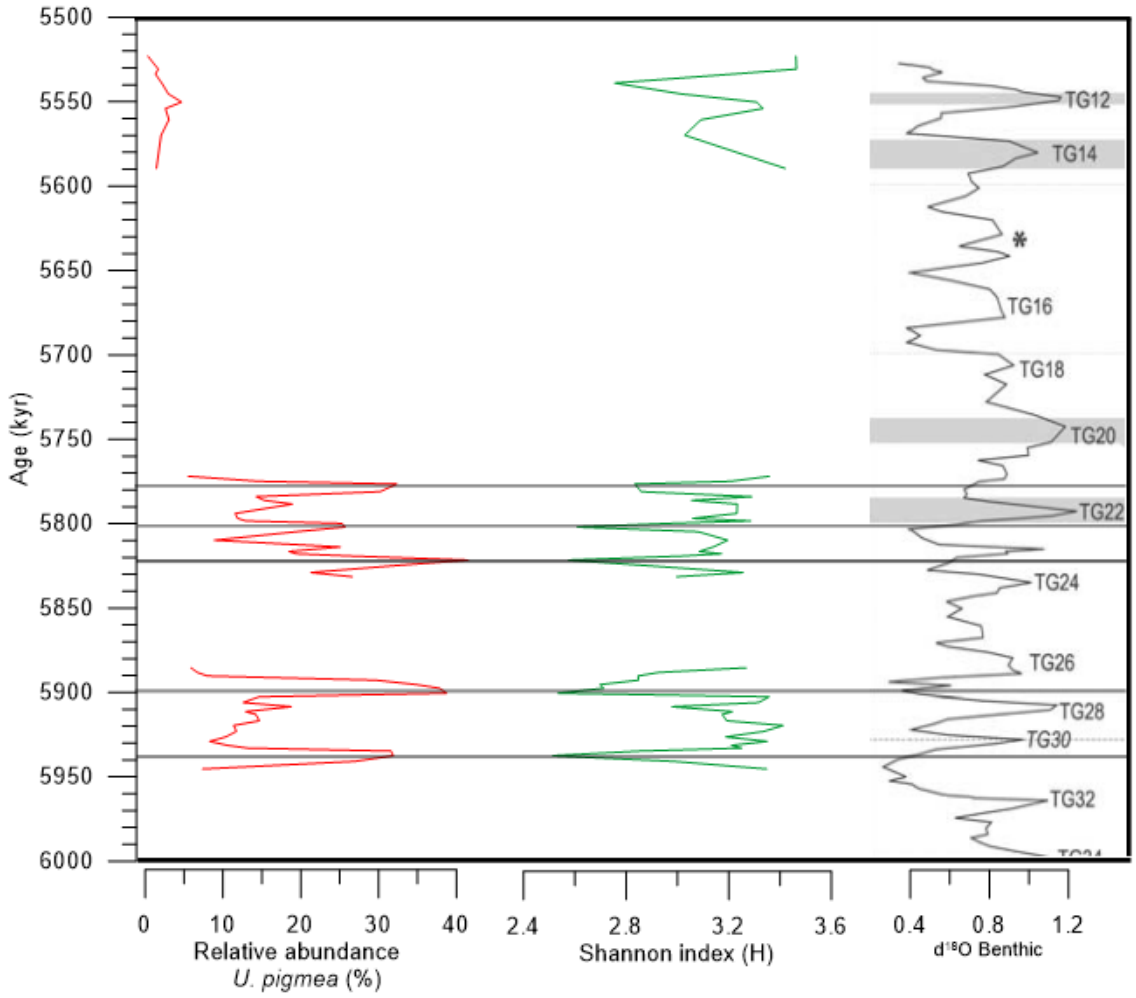

Fig. 17 – Comparison between the relative abundance of *U. pigmea*, the Shannon index and the benthic $\delta^{18}O$ record with added glacial intervals; TG12-32 (van der Laan et al., 2005).

Dominance of *U. pigmea* is related to increased organic flux and upwelling (Minagawa and Minagawa, 1997; Schönfeld and Altenbach 2005). The study of Schönfeld and Altenbach (2005) demonstrates that peak proportions of *U. pigmea* correlate directly to high amounts of upwelling-indicating planktonic foraminifera. Coastal upwelling is expected when alongshore winds are dominant (Martinez et al., 1999; Wang et al., 2015). Dominant winds and enhanced upwelling are often associated with glacials (Guichard et al, 1999; Schönfeld and Altenbach 2005). However, Figure 17 shows that the peak proportions of *U. pigmea* correlate to minima in the benthic $\delta^{18}O$ record of the Ain el Beida section, while maxima in benthic $\delta^{18}O$ correlate to glacial activity (van der Laan et al., 2005). The pattern of *U. pigmea* suggests that upwelling occurred prior to or succeeding glacials. Although there is common agreement on a global increase in upwelling during glacials, there are significant local differences (Martinez et al., 1999). In Northwest Africa, high summer monsoon intensity causes strong southward alongshore trade winds resulting in strong upwelling intensity (Martinez et al., 1999). The African summer monsoon strengthens during high seasonality (enhanced boreal summer insolation), i.e. precession minima and obliquity maxima (Larrasoaña et al., 2003; Tuenter et al., 2003). Monsoonal controlled upwelling in the Gharb basin during precession minima (i.e. red marl formation) therefore explains the dominance of *U. pigmea* in the red marls.

Figure 6 demonstrates a relatively low abundance of *U. pigmea* in the red marl of cycle 28. This marl is associated with a decreased insolation maxima related to a minimum in obliquity (Fig. 15). The minimum in obliquity probably results in decreased monsoonal strength. Consequently, upwelling is decreased. This explains the relatively low abundance of *U. pigmea*.

Upwelling can explain the relative increase of benthic foraminifera compared to planktonic foraminifera in the red marls, demonstrated by the P/B ratio (Fig. 16). Because the winds blows parallel to the coast, Ekman transport produces offshore surface currents in Northwest Africa. This results in an upwelling water mass that flows in opposite direction over the bottom of the ocean towards the coast; i.e. coastal upwelling (Wang et al., 2015). Consequently, the organic flux from the deeper parts of the ocean is preserved for the bottom of the ocean in the benthic ecosystem. This results in a relative increase of benthic foraminifera in the red marls. The species *U. pigmea* profits from this increased organic flux. The additional organic matter probably leads to increased oxygen consumption and degradation. This results in an increase in stress and a decrease in species diversity.

Besides upwelling, the relatively high sedimentation rate during red marl formation attributes to the increase in organic flux and dominance of *U. pigmea*. The additional supply of nutrients amplifies primary productivity in the surface waters and thereby increases the organic flux to the bottom waters. An extreme example of this can be found in the red marl of AEB 33 (Fig. 16). The sedimentation rate reaches a maximum value of 20 cm/kyr. Even in this highly diluted setting, the benthic foraminiferal counts increases to 350 per gram, indicating a strong growth in benthic biomass. The P/B ratio decreases to 50%, reflecting a relative increase of benthic foraminifera compared to planktonic foraminifera.

There is a strong relation between the distribution of the species of Groups 1 and 2 and lithology (Figs. 12, 15). The species *G. soldanii* and *O. umbonatus* of Group 2 are reduced in the red marls. They are not able to tolerate low-oxygen levels (Van der Zwaan and Den Hartog Jager, 1983). The species *C. pseudoungerianus* and *U. pigmea* are relatively more abundant in the red marls. *U. pigmea* (often referred as *U. peregrina* in literature) and *C. pseudoungerianus* are described to have a high tolerance towards lowered oxygen conditions (van der Zwaan, 1982; Murray, 1991, van de Poel et al., 1992). Besides upwelling and increased organic flux, high proportions of *U. pigmea* are also associated with decreased oxygen content (van der Zwaan, 1982, Loubère, 1996). However, the relatively high abundances of *C. pseudoungerianus* and *U. pigmea* also indicate that oxygen reduction in the red marls was not extreme (van der Zwaan, 1982; van de Poel et al., 1992).

The benthic foraminiferal assemblages show strong evidence that the red marls are associated with a reduction of oxygen content and an increase in organic flux through upwelling and sediment transport. The white marls are characterized by reoxygenation and reduced organic flux. Species that are not tolerant to lowered oxygen content are reduced in the red marls, but not absent. Furthermore, the species diversity is only slightly lowered. This shows that the bottom waters during the formation of red marls are not fully depleted of oxygen, but only somewhat reduced. Furthermore, the relatively high abundance of the species *C. pseudoungerianus* and *U. pigmea* indicate low-oxygen levels, but they also indicate that the environment was not anoxic (van der Zwaan, 1982; van de Poel et al., 1992).

5.3.2 Astronomically induced changes in humidity

The oxygen reduction in the red marls can be partly explained by the consuming and degradation of the additional organic matter. However, only five out of nine red marls display strong maxima in relative abundance of *U. pigmea* (Fig. 6). The relative abundance of *U. pigmea* in the red marls of the upper part of the section is very low, showing no evidence for upwelling. The species diversity and various benthic foraminiferal species indicate lower oxygen levels during the formation of all red marls. It remains uncertain if upwelling occurred during all red marl formation intervals. Furthermore, the magnitude of the increased organic flux and oxygen consumption is unclear. It is therefore unlikely that the perceived oxygen reduction during red marl formation is only the result of upwelling. The oxygen reduction during red marl formation can also be explained by enhanced stratification during red marl formation which reduces oxygen flux to the bottom waters.

This reduction in vertical mixing during red marl formation is probably related to increased humidity during precession minima. In this scenario increased humidity results in a stronger fresh water flux to the Gharb basin increasing stratification and decreasing ventilation of the bottom

waters. The precession signal mainly controls the regional climate in the Mediterranean region (Hilgen et al., 2007). The clear imprint of the precession signal in various proxies of the Ain el Beida section is probably the result of regional climate response to changes in precession (van der Laan et al., 2005). During enhanced seasonality related to mainly precession minima and secondarily obliquity maxima, conditions in Northwest Africa were more humid (Rossignol-Strick, 1983; Bosmans et al., 2015). The Ti/Al record of the Ain el Beida section indicates more humid conditions during red marl formation (van der Laan et al., 2012).

Model results show that during precession minima precipitation over the North-western African landmass increases, especially during summer. This is related to the enhanced influence of the African monsoon during precession minima (Bosmans et al., 2015). Furthermore, the model indicates that winter precipitation increased significantly over the Atlantic Ocean and Atlantic side of the Rifian Corridor during precession minima and obliquity maxima (Bosmans et al., 2015). Today, Atlantic depressions in winter give rain in the region of the Gharb basin (Knippertz et al., 2003). These depressions are likely to intensify during increased seasonality. However, Bosmans et al. (2015) states that stronger air-sea temperature differences are the main reason for the enhanced winter precipitation. The influence of the Atlantic system in the region of the Gharb basin is in agreement with studies that link the Atlantic depressions to climatic and environmental changes in Northwest Africa (Petit-Maire and Guo, 1997; Sierro et al., 1999; van der Laan et al., 2012).

Enhanced precipitation in summer during precession minima over Northwest Africa resulted in enhanced fluvial run-off and consequently stratification in the Gharb basin during red marl formation. Increased winter precipitation during enhanced seasonality (i.e. precession minima and obliquity maxima) over the Atlantic side of the Rifian Corridor contributed to the reduction in vertical circulation.

Red marls are associated with stratification leading to reduced vertical circulation and with upwelling. These processes probably did not occur simultaneously, because an upwelling water mass would cancel out stratification. It is likely that these two processes occurred during different periods in the year. Because upwelling is related to the African summer monsoon, it mainly occurs during summer. The reduction in vertical circulation would have happened between late summer and winter. This is because the increase in precipitation over land during summer related to the African monsoon would have increased the run-off during late summer and early autumn. The increase in winter precipitation over the Gharb basin related to the Atlantic system would have increased stratification during winter.

5.3.3 Sapropels and red marls

Both sapropels in the Mediterranean and red strata in the Rif Corridor are associated with reduced oxygen levels. Red marls and sapropels are both related to precession minima/summer insolation maxima and witness the same characteristic signal in quantitative planktonic foraminiferal analyses (e.g. maxima of Globigerinoides spp.) and stable isotope records ($\delta^{18}O$ minima) (Hilgen, 2000; Krijgsman et al., 2004). The benthic foraminiferal assemblages indicate a reduced vertical circulation and increased primary productivity during red marl formation. Sapropels are associated with reduced vertical circulation and increased primary productivity as well (Rossignol-Strick, 1985; Schmiedl et al., 2003; Tuenter et al., 2003). The red marls can be referred to as the 'light versions' of sapropels. The environmental fluctuations leading to the formation of red and light beige marls were not as extreme as sapropels and homogenous marls in Mediterranean sections. In contrast to several sapropels, conditions during red marl formation never became anoxic. This is clearly demonstrated by the benthic foraminiferal assemblages. This is also apparent from variations in planktonic and benthic $\delta^{18}O$ of the Ain El Beida section, which are less prominent compared to Mediterranean sections (van der Laan et al., 2012).

Figure 13 demonstrates that variations on sub-precessional scale in the composition of the benthic foraminiferal assemblages are common within the red marls. They are probably the result of intervals of short reoxygenation events. Various sapropels are also characterized with these

variations. There are intervals within Mediterranean sapropels S5 and S6 of the Neogene where the amount of benthic foraminifera is increased (Jorissen, 1999; Schmiedl et al., 2003; Morigi, 2009). This is interpreted as reoxygenation within a generally anoxic sapropel. This demonstrates that the deep water ventilation is sensitive to minor climate fluctuations on millennial scale, especially for lesser expressed sapropels (Schmiedl et al., 2003).

The similarity of red marls and Mediterranean sapropels suggests similar formation processes. The reduced bottom water ventilation during red marl and sapropel formation is the result of increased density differences between high-density bottom and low-density surface waters, reducing vertical mixing and causing stratified waters. As for sapropel formation, this occurs when precipitation increases due to the increased strength of the African summer monsoon during precession minima. The relatively high precipitation results in an increase in freshwater run-off by rivers resulting in a decrease in vertical mixing (Rossignol-Strick, 1985; Tuenter et al., 2003). This is also the case for red marls. However, the precipitation increase during red marl formation is also the result of the Atlantic system.

5.3.4 Salinity

The benthic foraminiferal assemblages indicate a depositional depth of the Ain el Beida between 600-1200m (Fig. 14). The benthic assemblages are in this case not an appropriate proxy to study salinity, because little is known about salinity markers on these depths (pers. comm.). Only some shelf taxa (0-100 m) such as *Ammonia spp.,* are known to thrive under high salinity conditions (Almogi-Labin et al., 1992). Moreover, the distribution of benthic foraminifera is mainly the result of the interaction between organic flux and oxygen content (TROX model, Jorrissen et al., 1995). The observed relation between lithology and benthic assemblages is therefore best explained by variations in oxygen level and organic flux. Reconstructing outflow of Mediterranean waters by salinity fluctuations is therefore not possible.

5.3.5 Outflow of Mediterranean waters

To accommodate for the amount of evaporites, water exchange between the Mediterranean Sea and Atlantic Ocean during the first stage of the MSC (i.e. deposition of lower evaporites) must have been present (Krijgsman et al., 1999b; Hilgen et al., 2007; Flecker et al., 2015). The interval of the first stage (5.97-5.60 Ma) coincides with the lower and middle part of the studied section (Fig. 15). Outflow of Mediterranean waters during precession minima (i.e. red marl formation) could result in stratified waters during red marl formation. In this scenario the denser, salter Mediterranean waters sink to the bottom of the Rifian Corridor changing the benthic ecosystem. The density contrast between bottom and surface waters would reduce vertical mixing and bottom water ventilation and thereby limiting oxygen availability.

The variability in Mediterranean outflow into the gateways is tectonically controlled but also modulated by astronomically induced density changes between the Mediterranean Sea and Atlantic Ocean (Flecker et al., 2015). The bathymetric reconstruction (Fig. 14) indicates a relatively stable depth of the Gharb basin during the first stage of the MSC, presumably allowing exchange and suggesting an astronomical control on Mediterranean outflow. A relative increase in evaporation compared to fluvial run-off and precipitation will result in an increase in salinity of the surface waters. Consequently, the denser surface waters will sink faster in the Eastern Mediterranean enhancing deep water formation. This increases basin-scale circulation and results in more exchange between Mediterranean and Atlantic waters (Flecker et al., 2015). This is expected during precession maxima (i.e. light beige marl formation), when the precipitation and run-off is relatively low because of the reduced summer insolation (Rossignol-Strick, 1985; Tuenter et al., 2003). However, the benthic foraminiferal assemblages indicate reduced vertical mixing during the formation of red marls instead of light beige marls. Therefore, outflow of Mediterranean waters probably did not contribute to the different environmental conditions leading to red and light beige marls.

The benthic assemblages in the upper part of the studied section are rather different in composition compared to the middle and lower part of the section (Figs. 8, 9). The interval of the upper part of the section coincides with the second stage of the MSC (5.60-5.55 Ma). During this most extreme part of the MSC the sea-level of the Mediterranean Sea declined rapidly because of extensive evaporation and possibly glacio-eustasy (Roveri et al., 2008; Manzi et al., 2013). The bathymetric reconstruction of this study indicates a sea-level lowering during the second stage as well (Fig. 14). This prevented outflow of Mediterranean waters into the Rifian Corridor (Flecker et al., 2015). The absence of Mediterranean outflow possibly attributes to the difference in the composition of the benthic foraminifera in the upper part of the section. In addition, the absence of exchange means that Mediterranean outflow did not influence the environmental conditions leading to the alternations of red and light beige marls in the upper part of the section.

It is not clear in what extend Mediterranean outflow influenced the composition of the benthic foraminifera during the first part of the MSC (lower and middle part of the section). The amount of outflow was probably not substantial, because parts of the Rifian Corridor were already emerged during the first stage of the MSC (Krijgsman et al., 1999c). Furthermore, Nd isotope records display restriction of the gateway prior to the onset of the MSC (Ivanovic et al., 2013).
Because of the high density, Mediterranean waters would sink to the deepest part of the Rifian Corridor. However, the location of the deepest part of the gateway is currently unknown (pers. comm.). The Ain el Beida section is located near the southern edge of the Rifian Corridor (Fig. 2). It is possible that Mediterranean water fluxes did not reach Ain el Beida because it did not belong to the deepest part of the gateway. Furthermore, The Ain el Beida section is located near the Atlantic Ocean (Fig. 2). Extensive mixing of Mediterranean waters could have occurred before the water mass reached the location of Ain el Beida.

6. Conclusions

In this study, benthic foraminifera have been used to reconstruct environmental changes in the Atlantic side of the Rifian Corridor during the first stages of the MSC. These are the most important results:

- The bathymetric reconstruction demonstrates a relatively stable paleodepth of the Gharb basin of approximately 1000 m during the first stage of the Miocene (5.95-5.77 Ma). A decreasing trend in sea-level is observed between 5.59-5.52 Ma. This shallowing of 200-300 m is interpreted to be the result of tectonic activity between Africa and Iberia. The decreasing trend in sea-level towards the end of the Miocene is observed in benthic foraminiferal studies of other sections in the Gharb basin as well. The shallowing interval coincides with the onset and duration of the second stage of the MSC (5.60-5.55 Ma). This study supports the notion that the extreme conditions during the second stage of the MSC are related to sea-level lowering resulting in complete isolation of the Mediterranean Sea.
- The benthic foraminiferal assemblages of the Ain el Beida section clearly show an astronomical signal related to the cyclic alternations of red and light beige marls. This is apparent from the benthic counts, P/B ratio, species diversity and statistical analysis on the assemblages. The composition of the benthic assemblages is mainly related to precession, modulated by eccentricity and with minor influence of obliquity.
- The composition of benthic foraminifera demonstrates that the red marls are associated with an increase in organic flux and a reduction in oxygen content. The light beige marls are associated with reoxygenation of the environment. The red marls show great similarity with Mediterranean sapropels. However, the benthic counts and the species diversity show that the environmental fluctuations in the Gharb basin were not as extreme as the environmental fluctuations leading to the alternations of homogeneous marls and sapropels in the Mediterranean sections.

- The distribution of the species *U. pigmea* indicates enhanced upwelling during red marl formation. This is explained by the increased strength and influence of the African monsoon during precession minima (i.e. red marl formation). The increased strength of the monsoon results in strong southward alongshore trade winds causing strong coastal upwelling. The relative increase in benthic foraminifera compared to planktonic foraminifera observed in the P/B ratio is a consequence of the enhanced upwelling. This is because the upwelling water mass transports old and deep organic matter over the bottom of the gateway in the benthic ecosystem. However, not all red marls are associated with upwelling. Furthermore, the consuming of oxygen related to upwelling is probably not sufficient to explain all the oxygen reduction during red marl formation.
- The reduction in oxygen levels during red marl formation is explained by increased stratification. The reduction in vertical mixing is not the result of outflow of denser Mediterranean waters because this is expected during precession maxima (i.e. light beige marl formation). Furthermore, during the second stage of the MSC no Mediterranean outflow is expected. The reduction in vertical mixing is best explained by increased fluvial run-off and precipitation during red marl formation. The red marls are linked in several studies to increased humidity. Model studies indicate increased precipitation and fluvial run-off during precession minima (i.e. red marl formation) over Northwest Africa. The reduction in vertical circulation and upwelling during red marl formation probably did not occur simultaneously because an upwelling water mass would cancel out stratification. These processes are seasonal and occurred probably in succession.
- The benthic foraminiferal assemblages do not show evidence for outflow of Mediterranean waters. However, according to several studies some exchange must have occurred during the first stage of the MSC. Because of the close location of Ain el Beida to the Atlantic Ocean and because the geometry of the Rifian Corridor is unknown, it is possible that fluxes of Mediterranean outflow did not influence the benthic ecosystem in Ain el Beida.

Acknowledgements

I would like to thank *dr. F.J. Hilgen* for choosing the right subject for this thesis that matched my interest. I would like to thank *dr. T.J. Kouwenhoven* particularly for helping with the identification of the benthic foraminiferal species, statistical analysis and for further assistance to the project.

References

Almogi-Labin, A., Perelis-Grossovicz, L., & Raab, M. (1992). Living Ammonia from a hypersaline inland pool, Dead Sea area, Israel. Journal of Foraminiferal Research, 22(3), 257-266.

Altenbach, A. V., Pflaumann, U., Schiebel, R., Thies, A., Timm, S., & Trauth, M. (1999). Scaling percentages and distributional patterns of benthic foraminifera with flux rates of organic carbon. Journal of Foraminiferal Research, 29(3), 173-185.

Barbieri, R., & Ori, G. G. (2000). Neogene palaeoenvironmental evolution in the Atlantic side of the Rifian Corridor (Morocco). Palaeogeography, Palaeoclimatology, Palaeoecology, 163 (1), 1-31.

Benson, R. H., Rakic-El Bied, K., and Bonaduce, G., (1991). An important current reversal (influx) in the Rifian Corridor (Morocco) at the Tortonian-Messinian boundary: The end of the Tethys ocean: Paleocanography,v. 6, p. 164–192.

Benson, R. H., Hayek, L. A. C., Hodell, D. A., & Bied, R. E. (1995). Extending the climatic precession curve back into the late Miocene by signature template comparison. Paleoceanography, 10(1), 5-20.

Berggren, W. A., & Miller, K. G. (1989). Cenozoic bathyal and abyssal calcareous benthic foraminiferal zonation. Micropaleontology 35, 308-320.

Clauzon, G., Suc, J. P., Gautier, F., Berger, A., & Loutre, M. F. (1996). Alternate interpretation of the Messinian salinity crisis: Controversy resolved?. Geology, 24(4), 363-366.

De Rijk, S., Jorissen, F. J., Rohling, E. J., & Troelstra, S. R. (2000). Organic flux control on bathymetric zonation of Mediterranean benthic foraminifera. Marine Micropaleontology, 40(3), 151-166.

De Stigter, H. C., Jorissen, F. J., & Van der Zwaan, G. J. (1998). Bathymetric distribution and microhabitat partitioning of live (Rose Bengal stained) benthic foraminifera along a shelf to bathyal transect in the southern Adriatic Sea. The Journal of Foraminiferal Research, 28(1), 40-65.

Esteban, M., Braga, J.C., Martin, J., de Santisteban, C., (1996). Western Mediterranean reef complexes - Models for Carbonate Stratigraphy from Miocene Reef Complexes of Mediterranean Regions. SEPM Concepts Sedimentology Paleontology. 5, 55–72.

Flecker, R., Krijgsman, W., Capella, W., de Castro Martíns, C., Dmitrieva, E., Mayser, J.P., Marzocchi, A., Modestou, S., Ochoa, D., Simon, D., Tulbure, M., van den Berg, B., van der Schee, M., de Lange, G., Ellam, R., Govers, R., Gutjahr, M., Hilgen, F., Kouwenhoven, T., Lofi, J., Meijer, P., Sierro, F.J., Bachiri, N., Barhoun, N., Alami, A.C., Chacon, B., Flores, J.A., Gregory, J., Howard, J., Lunt, D., Ochoa, M., Pancost, R., Vincent, S., Yousfi, M.Z. (2015). Evolution of the Late Miocene Mediterranean– Atlantic gateways and their impact on regional and global environmental change. Earth-Science Reviews 150, 365–392

Garcia-Castellanos, D., Estrada, F., Jiménez-Munt, I., Gorini, C., Fernández, M., Vergés, J., & De Vicente, R. (2009). Catastrophic flood of the Mediterranean after the Messinian salinity crisis. Nature, 462(7274), 778-781.

Guichard, S., Jorissen, F., & Peypouquet, J. P. (1999). Late Quaternary benthic foraminiferal records testifying lateral variability of the Cape Blanc upwelling signal. Comptes Rendus de l'Académie des Sciences-Series IIA-Earth and Planetary Science, 329(4), 295-301.

Hammer, Ø., Harper, D.A.T., Ryan, P.D. (2001). PAST: Paleontological statistics software package for education and data analysis. Palaeontologia Electronica 4(1): 9pp.

Hansen, H. J. (1979). Test structure and evolution in the Foraminifera. Lethaia, 12(2), 173-182.

Herguera, J. C. (1992). Deep-sea benthic foraminifera and biogenic opal: glacial to postglacial productivity changes in the western equatorial Pacific. Marine Micropaleontology, 19(1), 79-98.

Hilgen, F. J., & Krijgsman, W. (1999). Cyclostratigraphy and astrochronology of the Tripoli diatomite formation (pre-evaporite Messinian, Sicily, Italy). Terra Nova-Oxford, 11(1), 16-22.

Hilgen, F. J., Bissoli, L., Iaccarino, S., Krijgsman, W., Meijer, R., Negri, A., & Villa, G. (2000). Integrated stratigraphy and astrochronology of the Messinian GSSP at Oued Akrech (Atlantic Morocco). Earth and Planetary Science Letters, 182(3), 237-251.

Hilgen, F. J., Kuiper, K., Krijgsman, W., Snel, E., & van der Laan, E. (2007). Astronomical tuning as the basis for high resolution chronostratigraphy: the intricate history of the Messinian Salinity Crisis. Stratigraphy, 4(2-3), 231-238.

Hodell, D. A., Curtis, J. H., Sierro, F. J., & Raymo, M. E. (2001). Correlation of late Miocene to early Pliocene sequences between the Mediterranean and North Atlantic. Paleoceanography, 16(2), 164-178

Hohenegger, J. (2005). Estimation of environmental paleogradient values based on presence/absence data: a case study using benthic foraminifera for paleodepth estimation. Palaeogeography, Palaeoclimatology, Palaeoecology, 217(1), 115-130.

Holbourn, A., Henderson, A. S., & MacLeod, N. (2013). Atlas of benthic foraminifera. John Wiley & Sons.

Hsü, K. J. (1972). Origin of saline giants: a critical review after the discovery of the Mediterranean evaporite. Earth-Science Reviews, 8 (4), 371-396.
Hsü, K. J. (1973). The desiccated deep-basin model for the Messinian events. Messinian Events in the Mediterranean. Geodynamics Scientific Report, (7), 2-4.
Hsü, K.J., Montadert, L., Bernoulli, D., Bianca Cita, M., Erickson, A., Garrison, R.E., Kidd, R.B., Mèlierés, F., Müller, C., & Wright, R., (1977). History of the Mediterranean salinity crisis. Nature 267,399–403.
Jorissen, F. J., de Stigter, H. C., & Widmark, J. G. (1995). A conceptual model explaining benthic foraminiferal microhabitats. Marine Micropaleontology, 26(1), 3-15.
Jorissen, F. J. (1999). Benthic foraminiferal successions across Late Quaternary Mediterranean sapropels. Marine Geology, 153(1), 91-101.
Knippertz, P., Christoph, M., & Speth, P. (2003). Long-term precipitation variability in Morocco and the link to the large-scale circulation in recent and future climates. Meteorology and Atmospheric Physics, 83(1-2), 67-88.
Kouwenhoven, T. J., F. Hilgen J., and Van der Zwaan G. J. (2003). Late Tortonian–early Messinian stepwise disruption of the Mediterranean–Atlantic connections: constraints from benthic foraminiferal and geochemical data. Palaeogeography, Palaeoclimatology, Palaeoecology 198.3 303-319.
Krijgsman, W., Hilgen, F. J., Marabini, S., & Vai, G. B. (1999a). New paleomagnetic and cyclostratigraphic age constraints on the Messinian of the Northern Apennines (Vena del Gesso Basin, Italy). Mem. Soc. Geol. It, 54, 25-33.
Krijgsman, W., Hilgen, F. J., Raffi, I., Sierro, F. J., & Wilson, D. S. (1999b). Chronology, causes and progression of the Messinian salinity crisis. Nature,400(6745), 652-655.
Krijgsman, W., Langereis, C. G., Zachariasse, W. J., Boccaletti, M., Moratti, G., Gelati, R., Villa, G. (1999c). Late Neogene evolution of the Taza–Guercif Basin (Rifian Corridor, Morocco) and implications for the Messinian salinity crisis. Marine Geology, 153(1), 147-160.
Krijgsman, W., Fortuin, A. R., Hilgen, F. J., & Sierro, F. J. (2001). Astrochronology for the Messinian Sorbas basin (SE Spain) and orbital (precessional) forcing for evaporite cyclicity. Sedimentary Geology, 140(1), 43-60.
Krijgsman, W., Blanc-Valleron, M. M., Flecker, R., Hilgen, F. J., Kouwenhoven, T. J., Merle, D., Orszag-Sperber, F., & Rouchy, J. M. (2002). The onset of the Messinian salinity crisis in the Eastern Mediterranean (Pissouri Basin, Cyprus). Earth and Planetary Science Letters, 194(3), 299-310.
Krijgsman, W., Gaboardi, S., Hilgen, F. J., Iaccarino, S., Kaenel, E. D., & Laan, E. V. D. (2004). Revised astrochronology for the Ain el Beida section (Atlantic Morocco): no glacio-eustatic control for the onset of the Messinian Salinity Crisis. Stratigraphy, 1, 87-101.
Langer, M. R. (1999). Origin of foraminifera: conflicting molecular and paleontological data?. Marine micropaleontology, 38(1), 1-5.
Larrasoaña, J. C., Roberts, A. P., Rohling, E. J., Winklhofer, M., & Wehausen, R. (2003). Three million years of monsoon variability over the northern Sahara. Climate Dynamics, 21(7-8), 689-698.
Laskar, J., Joutel, F., & Boudin, F. (1993). Orbital, precessional, and insolation quantities for the Earth from-20 Myr to+ 10 Myr. Astronomy and Astrophysics,270, 522-533.
Laskar, J., Robutel, P., Joutel, F., Gastineau, M., Correia, A. C. M., & Levrard, B. (2004). A long-term numerical solution for the insolation quantities of the Earth. Astronomy & Astrophysics, 428(1), 261-285.
Lear, C. H., Elderfield, H., & Wilson, P. A. (2000). Cenozoic deep-sea temperatures and global ice volumes from Mg/Ca in benthic foraminiferal calcite. Science, 287(5451), 269-272.
Lear, C. H., Elderfield, H., & Wilson, P. A. (2003). A Cenozoic seawater Sr/Ca record from benthic foraminiferal calcite and its application in determining global weathering fluxes. Earth and Planetary Science Letters, 208(1), 69-84.
Loubère, P. (1996). The surface ocean productivity and bottom water oxygen signals in deep water benthic foraminiferal assemblages. Marine Micropaleontology, 28(3-4), 247-261.
Lozar, F., Violanti, D., Pierre, F. D., Bernardi, E., Cavagna, S., Clari, P., , P., Irace, A., Martinetto, E., & Trenkwalder, S. (2010). Calcareous nannofossils and foraminifers herald the Messinian salinity crisis: the Pollenzo section (Alba, Cuneo; NW Italy). Geobios, 43(1), 21-32.
Maillard, A., Gorini, C., Mauffret, A., Sage, F., Lofi, J., & Gaullier, V. (2006). Offshore evidence of polyphase erosion in the Valencia Basin (Northwestern Mediterranean): scenario for the Messinian Salinity Crisis. Sedimentary Geology, 188, 69-91.
Martinez, P., Bertrand, P., Shimmield, G. B., Cochrane, K., Jorissen, F. J., Foster, J., & Dignan, M. (1999). Upwelling intensity and ocean productivity changes off Cape Blanc (northwest Africa) during the last 70,000 years: geochemical and micropalaeontological evidence. Marine Geology, 158(1), 57-74.

Meijer, P. T., & Tuenter, E. (2007). The effect of precession-induced changes in the Mediterranean freshwater budget on circulation at shallow and intermediate depth. Journal of Marine Systems, 68(3), 349-365.
Minagawa, W., Minagawa, M., 1997. Response of benthic foraminifera to organic carbon accumulation rates in the Okinawa Trough. Journal of Oceanography 53, 411 – 420.
Morigi, C. (2009). Benthic environmental changes in the Eastern Mediterranean Sea during sapropel S5 deposition. Palaeogeography, Palaeoclimatology, Palaeoecology, 273(3), 258-271.
Murray. J.W., 1991. Ecology and Paleoecology of Benthic Foraminifera. Longman, Harlow.
Ogniben, L. (1957). Petrografia della Serie Solfifera Siciliana e considerazioni geologiche relative. Memorie Descriptive della Carta Geologica d'Italia 33, 1–275
Pawlowski, J., Holzmann, M., Berney, C., Fahrni, J., Gooday, A. J., Cedhagen, T., Habura, A., & Bowser, S. S. (2003). The evolution of early Foraminifera. Proceedings of the National Academy of Sciences, 100(20), 11494-11498.
Pérez-Asensio, J. N., Aguirre, J., Schmiedl, G., & Civis, J. (2012). Messinian paleoenvironmental evolution in the lower Guadalquivir Basin (SW Spain) based on benthic foraminifera. Palaeogeography, Palaeoclimatology, Palaeoecology, 326, 135-151.
Petit-Maire, N., and Z. Guo (1997), Holocene precipitation over the present-day Sahara desert: Implications for the future, Episodes, 20, 232– 234
Pierre, F. D., Bernardi, E., Cavagna, S., Clari, P., Gennari, R., Irace, A., Lozar, F., Lugli, S., Manzi, V., Natalicchio, M., Roveri, M., & Violanti, D., (2011). The record of the Messinian salinity crisis in the Tertiary Piedmont Basin (NW Italy): the Alba section revisited. Palaeogeography, Palaeoclimatology, Palaeoecology, 310(3), 238-255.
Raffi, I., Mozzato, C., Fornaciari, E., Hilgen, F. J., & Rio, D. (2003). Late Miocene calcareous nannofossil biostratigraphy and astrobiochronology for the Mediterranean region. Micropaleontology, 49(1), 1-26.
Ravelo, A. C., & Hillaire-Marcel, C. (2007). Chapter Eighteen the use of oxygen and carbon isotopes of foraminifera in Paleoceanography. Developments in Marine Geology, 1, 735-764.
Rossignol-Strick, M. (1985). Mediterranean Quaternary sapropels, an immediate response of the African monsoon to variation of insolation. Palaeogeography, palaeoclimatology, palaeoecology, 49(3), 237-263.
Rouchy, J. M., & Caruso, A. (2006). The Messinian salinity crisis in the Mediterranean basin: a reassessment of the data and an integrated scenario. Sedimentary Geology, 188, 35-67.
Roveri, M., Bertini, A., Cosentino, D., Di Stefano, A., Gennari, R., Gliozzi, E., . Grossi, F., Iaccarino, S.M., Lugli, S., Manzi, V., & Taviani, M. (2008). A high-resolution stratigraphic framework for the latest Messinian events in the Mediterranean area. Stratigraphy, 5(3-4), 323-342.
Roveri, M., Flecker, R., Krijgsman, W., Lofi, J., Lugli, S., Manzi, V., Sierro, F.J., Bertini, A., Carnerlenghi, A., De Lange, G., Govers, R., Hilgen, F.J., Huebscher, C., Meijer, P.T., & Stoica, M., (2014). The Messinian Salinity Crisis: past and future of a great challenge for marine sciences. Marine Geology, 352, 25-58.
Ryan, W. B. F., Hsü, K. J., et al. (1973). Leg 13. Initial Reports of the Deep Sea Drilling Project, 13, 1-1447.
Ryan, W. B. (1978). Messinian badlands on the southeastern margin of the Mediterranean Sea. Marine Geology, 27(3), 349-363.
Ryan, W. B. (2009). Decoding the Mediterranean salinity crisis. Sedimentology, 56(1), 95-136.
Santisteban, C., & Taberner, C. (1983). Shallow marine and continental conglomerates derived from coral reef complexes after desiccation of a deep marine basin: the Tortonian-Messinian deposits of the Fortuna Basin, SE Spain. Journal of the Geological Society, 140(3), 401-411.
Schmiedl, G., Mitschele, A., Beck, S., Emeis, K. C., Hemleben, C., Schulz, H., Sperling, M., & Weldeab, S. (2003). Benthic foraminiferal record of ecosystem variability in the eastern Mediterranean Sea during times of sapropel S 5 and S 6 deposition. Palaeogeography, Palaeoclimatology, Palaeoecology, 190, 139-164.
Schönfeld, J., & Altenbach, A. V. (2005). Late Glacial to Recent distribution pattern of deep-water Uvigerina species in the north-eastern Atlantic. Marine Micropaleontology, 57(1), 1-24.
Seidenkrantz, M. S., Kouwenhoven, T. J., Jorissen, F. J., Shackleton, N. J., & Van der Zwaan, G. J. (2000). Benthic foraminifera as indicators of changing Mediterranean–Atlantic water exchange in the late Miocene. Marine Geology, 163(1), 387-407.
Selli, R., (1960). Il Messiniano Mayer-Eymar 1867. Proposta di un neostratotipo. Giornale di Geologia 28, 1–33.
Sierro, F. J., Flores, J. A., Civis, J., Gonza, J. A., & France, G. (1993). Late Miocene globorotaliid event-stratigraphy and biogeography in the NE-Atlantic and Mediterranean. Marine Micropaleontology, 21(1), 143-167.
Sierro, F. J., Flores, J. A., Zamarreno, I., Vazquez, A., Utrilla, R., Frances, G., Hilgen, F.J., & Krijgsman, W. (1999). Messinian climatic oscillations, astronomic cyclicity and reef growth in the western Mediterranean. Mar. Geol, 153, 137-146.

Sierro, F. J., Hilgen, F. J., Krijgsman, W., & Flores, J. A. (2001). The Abad composite (SE Spain): a Messinian reference section for the Mediterranean and the APTS. Palaeogeography, Palaeoclimatology, Palaeoecology, 168(1), 141-169.
Spellerberg, I. F., & Fedor, P. J. (2003). A tribute to Claude Shannon (1916–2001) and a plea for more rigorous use of species richness, species diversity and the 'Shannon–Wiener'Index. Global ecology and biogeography, 12(3), 177-179.
Tuenter, E., Weber, S. L., Hilgen, F. J., & Lourens, L. J. (2003). The response of the African summer monsoon to remote and local forcing due to precession and obliquity. Global and Planetary Change, 36(4), 219-235.
Van der Laan, E., Gaboardi, S., Hilgen, F. J., & Lourens, L. J. (2005). Regional climate and glacial control on high-resolution oxygen isotope records from Ain el Beida (latest Miocene, northwest Morocco): A cyclostratigraphic analysis in the depth and time domain. Paleoceanography, 20(1).
Van der Laan, E., Hilgen, F. J., Lourens, L. J., De Kaenel, E., Gaboardi, S., & Iaccarino, S. (2012). Astronomical forcing of Northwest African climate and glacial history during the late Messinian (6.5–5.5 Ma). Palaeogeography, Palaeoclimatology, Palaeoecology, 313, 107-126.
Van De Poel, H. M., Witte, L., Lissenberg, T., & Schuurman, H. (1992).Foraminiferal biostratigraphy and palaeoenvironments of the Miocene-Pliocene Carboneras-Nijar basin (SE Spain) (No. 102-103). Nationaal Natuurhistorisch Museum.
Van der Zwaan, G. J. (1982). Paleoecology of late Miocene Mediterranean foraminifera. Utrecht Micropaleontological Bulletins, 25.
Van der Zwaan, G. J., Jorissen, F. J., & De Stigter, H. C. (1990). The depth dependency of planktonic/benthic foraminiferal ratios: constraints and applications. Marine Geology, 95(1), 1-16.
Van der Zaan, G., & Jager, D. (1983). Paleoecology of Late Miocene Sicilian benthic foraminifera. Proceedings of the koninklijke nederlandse akademie van wetenschappen series b-palaeontology geology physics chemistry anthropology, 86(2), 211-223.
Van der Zwaan, G. J., Duijnstee, I. A. P., Den Dulk, M., Ernst, S. R., Jannink, N. T., & Kouwenhoven, T. J. (1999). Benthic foraminifers: proxies or problems?: a review of paleocological concepts. Earth-Science Reviews, 46(1), 213-236.
Van Hinsbergen, D. J. J., Kouwenhoven, T. J., & Van der Zwaan, G. J. (2005). Paleobathymetry in the backstripping procedure: Correction for oxygenation effects on depth estimates. Palaeogeography, Palaeoclimatology, Palaeoecology, 221(3), 245-265.
Van Morkhoven, F. P., Berggren, W. A., Edwards, A. S., & Oertli, H. J. (1986). Cenozoic cosmopolitan deep-water benthic foraminifera (Vol. 11). Elf Aquitaine.
Wang, D., Gouhier, T. C., Menge, B. A., & Ganguly, A. R. (2015). Intensification and spatial homogenization of coastal upwelling under climate change. Nature, 518(7539), 390-394.

Appendix

1. *Counts of the benthic foraminifera of the Ain el Beida section*

sample	Lithology	Stratigraphy	Amphicoryna sp.	Anomalina colligera	Anomalina grossorugosa	Anomalina helicina	Anomalina spp.	Astrononion sp.	Bolivina dilatata	Bolivina hebes	Bolivina reticulata	Brizalina alata	Brizalina sp.	Bulimina aculeata	Bulimina striata	Bulimina striata mexicana	Cancris oblongus	Cassidulina sp.	Cassidulinoides sp.	Chilostomella sp.	Cibicides lobatus
AEB 269	MID RED 44	71.28 m	2	0	1	0	0	10	13	0	11	2	3	12	4	3	2	2	0	1	2
AEB 266	MID WHITE 43	70.18 m	1	0	0	1	0	17	52	6	24	0	4	30	1	1	3	0	1	0	16
AEB 264	BOT WHITE 43	69.82 m	0	1	1	3	0	4	19	0	13	0	2	19	6	1	0	0	0	0	1
AEB 262	MID RED 43	69.20 m	1	0	0	0	0	0	25	0	0	1	0	21	2	0	0	0	2	0	0
AEB 259	BOT RED 43	68.50 m	4	1	0	5	0	1	27	0	2	0	1	26	57	3	3	0	0	2	0
AEB 257	MID WHITE 42	67.99 m	3	2	1	3	0	1	25	0	2	0	2	21	87	5	1	0	0	0	5
AEB 256	BOT WHITE 42	67.56 m	2	1	0	0	0	1	6	0	8	1	1	23	20	0	1	2	1	0	0
AEB 254	MID RED 42	66.80 m	2	0	0	0	0	6	4	0	2	2	0	28	5	4	1	47	0	1	0
AEB 252	BOT RED 42	66.19 m	4	0	0	0	0	4	4	0	5	0	2	11	15	0	2	82	2	0	2
AEB 248	MID WHITE 41	64.90 m	2	1	0	2	0	7	3	0	3	1	1	24	11	0	1	5	0	0	1
AEB 210	TOP WHITE 34	53.38 m	2	1	1	1	1	5	5	5	7	0	0	26	7	0	1	0	1	0	1
AEB 209	MID WHITE 34	53.19 m	0	4	0	0	0	2	3	4	4	0	1	28	23	0	1	0	0	0	2
AEB 208	BOT WHITE 34	53.04 m	2	0	0	1	0	1	1	2	1	0	1	15	7	0	0	0	0	0	5
AEB 207	TOP RED 34	52.63 m	0	0	0	0	1	4	5	2	2	0	0	31	2	0	0	0	1	1	3
AEB 206	MID RED 34	52.36 m	5	0	0	3	0	2	6	5	4	0	3	43	3	0	2	0	1	2	4
AEB 205	MID RED 34	52.12 m	1	0	1	2	0	2	1	4	3	1	3	38	2	0	1	0	0	0	4
AEB 204	BOT RED 34	51.88 m	1	0	0	1	0	0	3	2	3	2	0	24	8	1	0	0	2	0	2
AEB 203	TOP WHITE 33	51.27 m	2	0	0	0	0	4	2	9	0	2	2	17	42	0	0	0	0	0	0
AEB 202	MID WHITE 33	50.88 m	0	1	0	1	0	1	7	24	16	0	1	27	29	0	0	0	0	0	3
AEB 201	BOT WHITE 33	50.58 m	1	1	0	2	0	1	1	14	9	0	3	18	32	0	0	0	1	0	2
AEB 200	TOP RED 33	50.29 m	0	2	0	1	0	1	2	17	12	1	2	25	31	0	2	0	1	0	1
AEB 199	MID RED 33	49.88 m	3	0	0	0	0	2	2	18	89	0	0	15	16	0	0	0	0	0	1
AEB 198	MID RED 33	49.34 m	0	1	0	0	0	0	4	31	18	0	2	29	4	0	5	0	1	2	1
AEB 197	MID RED 33	48.75 m	0	1	0	0	0	6	2	7	19	0	0	11	3	0	5	0	0	1	0
AEB 196	BOT RED 33	48.30 m	0	0	0	1	0	12	1	6	12	0	4	20	8	0	1	0	3	0	1
AEB 171	TOP WHITE 32	48.00 m	1	0	0	2	0	1	2	2	4	0	0	19	9	0	0	0	0	0	4
AEB 170	MID WHITE 32	47.87 m	0	2	0	1	0	1	3	9	9	1	0	24	16	3	1	0	0	0	1
AEB 169	BOT WHITE 32	47.75 m	2	0	0	1	0	2	0	4	3	0	1	12	9	1	0	0	1	0	0
AEB 168	TOP RED 32	47.54 m	0	0	0	0	0	1	2	4	4	0	1	19	3	1	0	0	1	2	2
AEB 167	MID RED 32	47.26 m	2	0	0	1	0	1	0	6	7	0	1	27	3	1	1	0	1	0	1
AEB 166	MID RED 32	46.95 m	1	0	0	0	0	2	2	3	2	0	0	15	5	0	1	0	3	0	4
AEB 165	BOT RED 32	46.78 m	1	0	2	1	0	7	1	4	3	1	1	33	8	0	3	0	2	0	5
AEB 150	TOP WHITE 29	43.86 m	0	0	0	0	0	3	1	3	2	1	0	22	23	0	0	0	1	0	2
AEB 149	MID WHITE 29	43.68 m	1	0	1	2	0	0	2	2	5	0	1	27	73	0	1	0	1	0	2
AEB 148	BOT WHITE 29	43.42 m	0	0	1	1	0	1	2	0	4	0	0	14	55	0	0	0	0	0	3
AEB 147	TOP RED 29	43.11 m	1	1	0	1	0	2	0	11	6	0	0	27	7	0	1	0	1	0	0
AEB 146	TOP RED 29	42.78 m	0	1	0	0	0	4	8	13	10	0	1	21	1	0	1	0	3	3	0
AEB 145	MID RED 29	42.52 m	3	0	0	1	0	6	5	3	6	0	3	21	7	0	0	0	2	0	1
AEB 144	MID RED 29	42.21 m	0	0	0	0	0	4	2	13	0	1	0	24	3	0	1	0	0	0	2
AEB 143	BOT RED 29	41.99 m	3	0	0	0	0	3	6	2	0	0	3	21	9	0	4	0	4	0	1
AEB 142	BOT RED 29	41.64 m	1	0	0	2	1	4	14	5	3	1	1	29	7	0	0	0	1	1	2
AEB 141	TOP WHITE 28	41.39 m	1	0	0	1	0	3	0	4	0	0	0	37	13	0	0	0	0	3	7
AEB 140	MID WHITE 28	41.08 m	1	0	0	0	0	2	1	0	12	1	0	24	28	0	1	0	1	0	0
AEB 139	BOT WHITE 28	40.84 m	3	0	0	1	0	2	4	2	2	0	0	21	10	0	1	0	0	0	0
AEB 138	TOP RED 28	40.32 m	2	0	0	1	0	0	0	2	3	0	0	33	5	1	0	0	2	0	0
AEB 137	MID RED 28	39.96 m	2	0	0	0	0	5	2	6	13	0	4	17	11	0	0	0	0	0	1
AEB 136	MID RED 28	39.66 m	1	0	0	0	0	25	5	9	41	1	8	25	16	0	3	0	0	0	3
AEB 135	BOT RED 28	39.38 m	3	3	0	1	0	2	0	2	7	0	3	27	3	0	6	0	0	1	0
AEB 134	MID WHITE 27	39.15 m	0	1	0	1	0	2	3	34	9	0	1	39	6	0	2	0	3	0	4
AEB 133	MID WHITE 27	38.95 m	1	4	0	0	0	0	9	12	14	0	1	28	6	0	0	0	1	0	1
AEB 132	TOP RED 27	38.81 m	1	1	0	0	0	4	5	15	10	1	0	22	2	0	0	0	1	1	1
AEB 131	TOP RED 27	38.65 m	1	1	0	1	0	3	3	3	4	0	2	29	2	1	0	0	2	0	1
AEB 130	MID RED 27	38.41 m	1	0	0	2	0	4	2	0	0	0	1	30	3	0	0	0	1	0	0
AEB 129	MID RED 27	38.13 m	3	3	0	1	0	2	2	3	5	0	1	28	7	0	2	0	0	0	2
AEB 128	BOT RED 27	37.82 m	2	0	0	0	0	10	2	11	24	1	4	9	9	0	2	0	4	0	1

sample	Lithology	Stratigraphy	Cibicidoides dutemplei	Cibicidoides incrassatus	Cibicidoides juvenile	Cibicidoides kullenbergi	Cibicidoides mundulus	Cibicidoides pachyderma	Cibicidoides pseudoungerianus	Cibicidoides spp.	Cibicidoides ungerianus	Elphidium crispum	Epistominella sp.	Eponides sp.	Fissurina sp.	Gavelinopsis lobatulus	Globobulimina sp.	Globocassidulina subglobosa	Guttulina sp.	Gyroidina soldanii	Hanzawaia boueana
AEB 269	MID RED 44	71.28 m	5	0	2	18	0	44	7	1	6	0	1	0	0	1	4	17	0	8	10
AEB 266	MID WHITE 43	70.18 m	10	11	1	25	2	28	9	4	14	0	1	1	1	0	0	20	0	10	9
AEB 264	BOT WHITE 43	69.82 m	5	0	4	5	0	45	2	3	3	0	0	0	1	1	0	9	0	1	5
AEB 262	MID RED 43	69.20 m	0	0	0	8	0	33	2	1	2	0	0	0	0	1	2	12	0	6	1
AEB 259	BOT RED 43	68.50 m	11	2	1	8	3	70	14	1	9	0	1	0	3	3	3	11	0	21	5
AEB 257	MID WHITE 42	67.99 m	5	9	2	1	3	12	10	1	10	0	3	0	2	3	1	9	1	4	5
AEB 256	BOT WHITE 42	67.56 m	3	3	1	2	0	19	7	5	7	0	0	0	0	0	0	3	0	5	5
AEB 254	MID RED 42	66.80 m	1	0	3	1	0	59	15	1	13	0	0	0	0	0	3	3	0	47	6
AEB 252	BOT RED 42	66.19 m	1	0	4	4	1	21	5	2	1	0	1	0	1	2	0	4	0	18	1
AEB 248	MID WHITE 41	64.90 m	0	4	2	3	0	37	2	2	8	2	0	0	0	2	0	8	1	10	6
AEB 210	TOP WHITE 34	53.38 m	0	7	2	7	2	22	0	0	1	0	0	0	2	0	0	8	0	3	7
AEB 209	MID WHITE 34	53.19 m	0	6	2	4	4	24	0	1	6	0	0	3	3	0	0	15	0	3	9
AEB 208	BOT WHITE 34	53.04 m	0	2	4	3	2	13	2	0	2	0	0	1	1	0	0	7	0	0	2
AEB 207	TOP RED 34	52.63 m	0	7	3	13	1	40	3	0	3	0	0	2	1	1	0	8	0	6	2
AEB 206	MID RED 34	52.36 m	0	1	7	9	1	37	16	0	4	0	1	0	1	0	1	4	0	4	8
AEB 205	MID RED 34	52.12 m	0	3	3	5	0	55	2	0	2	0	0	1	3	1	0	1	0	6	6
AEB 204	BOT RED 34	51.88 m	3	3	1	10	0	29	4	0	2	1	1	0	2	4	0	4	0	4	5
AEB 203	TOP WHITE 33	51.27 m	0	4	3	3	2	15	7	0	4	0	0	1	1	2	1	1	0	6	7
AEB 202	MID WHITE 33	50.88 m	0	5	0	4	1	19	0	0	0	0	0	0	0	0	0	3	0	6	5
AEB 201	BOT WHITE 33	50.58 m	1	4	4	7	3	13	4	1	1	0	0	1	2	0	0	5	0	3	6
AEB 200	TOP RED 33	50.29 m	0	7	2	5	2	12	10	0	0	0	0	1	0	0	0	6	1	1	4
AEB 199	MID RED 33	49.88 m	1	1	3	5	0	21	1	0	1	0	0	0	2	1	0	1	1	1	2
AEB 198	MID RED 33	49.34 m	0	3	5	10	0	53	14	0	15	0	3	0	1	1	1	0	0	2	2
AEB 197	MID RED 33	48.75 m	0	0	2	4	0	31	2	2	2	0	0	0	0	1	0	3	0	7	1
AEB 196	BOT RED 33	48.30 m	2	1	1	9	1	20	2	1	2	0	0	0	1	0	1	4	0	4	2
AEB 171	TOP WHITE 32	48.00 m	0	7	0	0	3	17	0	2	4	0	0	0	1	0	0	2	0	2	4
AEB 170	MID WHITE 32	47.87 m	2	9	13	6	2	38	7	0	7	0	0	1	1	0	0	9	0	6	11
AEB 169	BOT WHITE 32	47.75 m	0	3	2	2	4	12	0	1	3	0	0	2	0	0	0	2	0	6	3
AEB 168	TOP RED 32	47.54 m	0	1	2	4	3	23	2	0	2	0	0	3	1	0	1	0	0	1	1
AEB 167	MID RED 32	47.26 m	1	7	5	5	1	26	6	3	5	0	0	0	1	0	1	0	0	1	3
AEB 166	MID RED 32	46.95 m	0	0	2	6	0	15	9	3	4	0	0	0	1	1	0	1	0	5	3
AEB 165	BOT RED 32	46.78 m	0	4	0	4	3	18	1	2	0	0	0	0	1	0	1	2	0	1	1
AEB 150	TOP WHITE 29	43.86 m	5	3	2	15	1	23	3	0	3	0	1	0	1	0	0	3	0	4	4
AEB 149	MID WHITE 29	43.68 m	0	0	3	6	1	17	3	7	4	0	0	0	0	0	0	6	0	3	8
AEB 148	BOT WHITE 29	43.42 m	2	0	0	6	1	14	1	2	0	0	0	0	2	0	0	2	0	3	4
AEB 147	TOP RED 29	43.11 m	1	0	0	12	1	34	9	2	9	0	0	0	0	0	0	2	0	0	4
AEB 146	TOP RED 29	42.78 m	0	0	1	6	0	31	3	2	1	0	0	0	0	0	1	2	1	1	4
AEB 145	MID RED 29	42.52 m	1	0	4	18	0	35	4	0	3	0	1	0	0	0	4	1	0	1	8
AEB 144	MID RED 29	42.21 m	0	0	1	4	0	43	4	3	7	0	1	0	0	0	3	3	0	0	3
AEB 143	BOT RED 29	41.99 m	3	0	0	12	0	14	5	0	3	0	0	0	2	1	2	1	0	1	3
AEB 142	BOT RED 29	41.64 m	2	1	0	10	0	34	5	0	4	0	1	0	0	0	1	1	0	1	3
AEB 141	TOP WHITE 28	41.39 m	1	0	0	4	1	28	3	0	1	0	0	1	1	1	0	2	0	4	3
AEB 140	MID WHITE 28	41.08 m	0	0	1	12	0	6	1	1	5	0	1	0	2	0	0	3	0	7	2
AEB 139	BOT WHITE 28	40.84 m	3	0	0	5	0	26	2	0	3	0	0	0	2	0	0	3	0	3	1
AEB 138	TOP RED 28	40.32 m	1	0	0	7	2	16	2	0	3	0	0	0	0	0	0	1	0	4	3
AEB 137	MID RED 28	39.96 m	0	0	1	10	0	13	6	0	6	1	0	0	1	0	1	7	0	6	10
AEB 136	MID RED 28	39.66 m	4	0	1	18	0	14	3	2	3	1	0	0	1	0	0	7	0	6	15
AEB 135	BOT RED 28	39.38 m	0	0	0	7	1	43	4	1	9	0	0	0	0	0	0	4	0	4	5
AEB 134	MID WHITE 27	39.15 m	0	1	1	20	3	28	2	2	3	0	1	0	1	0	0	6	0	5	5
AEB 133	MID WHITE 27	38.95 m	1	0	4	14	0	28	4	1	6	0	0	1	0	0	0	18	0	5	5
AEB 132	TOP RED 27	38.81 m	0	1	0	6	0	22	3	0	2	0	0	0	0	0	0	11	0	6	1
AEB 131	TOP RED 27	38.65 m	1	0	2	13	0	23	2	0	6	0	0	0	1	0	0	3	0	0	4
AEB 130	MID RED 27	38.41 m	0	0	0	9	1	35	9	0	2	0	0	0	0	0	0	8	0	1	2
AEB 129	MID RED 27	38.13 m	1	1	1	5	1	24	6	2	3	2	0	0	0	0	0	10	0	3	7
AEB 128	BOT RED 27	37.82 m	2	0	1	3	0	4	0	2	1	3	0	0	1	0	0	5	0	6	13

sample	Lithology	Stratigraphy	Hanzawaia nipponica	Haplophragmoides sp.	Karreriella bradyi	Lagena sp.	Lenticulina sp.	Marginulina sp.	Martinotiella communis	Melonis barleeanus	Melonis soldanii	Neolenticulina sp.	Nodosaria sp.	Nonionella sp.	Oridorsalis umbonatus	Other agglutinated	other milliolids	Planulina ariminensis	Planulina spp.	Plectofrondicularia vaughani	Pseudonodosaria sp.
AEB 269	MID RED 44	71.28 m	4	0	2	3	12	0	0	10	6	0	3	0	0	2	2	0	0	0	2
AEB 266	MID WHITE 43	70.18 m	11	0	0	2	10	2	0	10	0	1	3	0	2	0	0	41	0	0	6
AEB 264	BOT WHITE 43	69.82 m	3	0	1	3	6	0	0	9	3	0	2	0	0	0	1	11	0	0	2
AEB 262	MID RED 43	69.20 m	2	0	4	2	17	0	0	2	0	1	2	0	2	2	0	2	0	0	2
AEB 259	BOT RED 43	68.50 m	0	0	2	4	14	1	0	12	4	0	5	1	14	0	0	16	1	2	10
AEB 257	MID WHITE 42	67.99 m	1	1	4	0	7	2	1	4	11	0	2	0	5	0	0	23	1	0	7
AEB 256	BOT WHITE 42	67.56 m	3	0	1	3	9	0	1	9	5	0	1	0	2	2	0	34	0	0	6
AEB 254	MID RED 42	66.80 m	0	0	3	3	12	0	1	4	14	0	0	0	1	2	2	37	0	0	2
AEB 252	BOT RED 42	66.19 m	2	0	1	0	14	1	0	3	1	0	2	0	2	2	0	24	0	0	5
AEB 248	MID WHITE 41	64.90 m	0	0	2	2	11	2	4	8	2	0	2	0	1	0	2	32	0	0	8
AEB 210	TOP WHITE 34	53.38 m	0	0	0	0	9	0	0	4	3	0	0	0	10	2	0	9	0	0	3
AEB 209	MID WHITE 34	53.19 m	0	0	0	0	12	1	0	3	2	0	1	0	10	2	0	21	0	0	3
AEB 208	BOT WHITE 34	53.04 m	0	0	2	0	10	0	0	1	1	0	2	0	6	0	0	13	0	0	3
AEB 207	TOP RED 34	52.63 m	0	0	1	4	14	1	1	0	5	0	5	0	4	0	1	22	0	0	4
AEB 206	MID RED 34	52.36 m	0	0	1	0	11	2	1	8	7	2	4	0	2	0	0	24	0	1	6
AEB 205	MID RED 34	52.12 m	0	0	1	1	14	2	1	3	8	2	5	0	2	0	0	25	0	0	4
AEB 204	BOT RED 34	51.88 m	0	0	0	0	14	2	1	12	16	1	6	0	0	0	1	22	0	0	4
AEB 203	TOP WHITE 33	51.27 m	0	0	0	4	11	6	0	6	12	3	5	0	5	0	0	23	0	0	9
AEB 202	MID WHITE 33	50.88 m	0	0	0	2	5	0	1	1	0	0	2	0	4	2	0	14	1	0	6
AEB 201	BOT WHITE 33	50.58 m	1	0	0	2	4	0	0	1	0	2	4	0	3	0	0	13	0	0	6
AEB 200	TOP RED 33	50.29 m	0	0	0	0	7	2	1	3	0	0	4	0	2	0	0	10	0	0	10
AEB 199	MID RED 33	49.88 m	2	0	0	2	7	0	3	2	4	0	3	0	0	0	1	17	0	2	3
AEB 198	MID RED 33	49.34 m	0	0	0	1	22	3	1	12	11	5	4	1	6	0	2	18	0	0	4
AEB 197	MID RED 33	48.75 m	3	0	0	1	4	0	0	6	6	0	2	1	0	0	1	7	0	0	0
AEB 196	BOT RED 33	48.30 m	0	0	0	2	7	2	0	5	1	0	4	0	1	1	0	14	0	0	4
AEB 171	TOP WHITE 32	48.00 m	0	0	0	3	15	0	0	0	0	0	4	0	5	0	0	17	0	0	4
AEB 170	MID WHITE 32	47.87 m	0	0	0	1	14	0	1	2	1	1	4	0	13	0	1	47	0	0	8
AEB 169	BOT WHITE 32	47.75 m	0	0	0	2	9	2	0	6	0	0	1	0	6	1	0	18	0	0	0
AEB 168	TOP RED 32	47.54 m	2	0	4	1	7	0	1	2	1	0	2	0	2	1	0	13	0	0	3
AEB 167	MID RED 32	47.26 m	0	0	5	0	14	0	2	5	2	0	2	0	2	1	0	12	0	1	9
AEB 166	MID RED 32	46.95 m	0	0	0	2	8	2	3	3	3	0	2	0	1	0	0	11	0	1	2
AEB 165	BOT RED 32	46.78 m	1	0	0	0	11	4	0	2	1	0	6	0	2	0	0	24	0	0	5
AEB 150	TOP WHITE 29	43.86 m	6	0	0	0	6	2	1	4	0	0	2	0	4	1	0	16	0	0	4
AEB 149	MID WHITE 29	43.68 m	3	0	0	0	5	2	0	4	0	0	4	0	5	0	0	22	0	0	2
AEB 148	BOT WHITE 29	43.42 m	3	0	0	1	3	0	0	3	1	0	3	0	1	2	0	18	1	0	3
AEB 147	TOP RED 29	43.11 m	0	0	0	2	13	1	1	7	6	0	2	0	2	2	2	19	0	0	0
AEB 146	TOP RED 29	42.78 m	0	0	0	1	7	1	0	2	4	0	3	1	0	2	1	10	0	0	0
AEB 145	MID RED 29	42.52 m	0	0	3	0	21	7	0	5	9	0	5	0	1	1	2	15	0	0	3
AEB 144	MID RED 29	42.21 m	0	0	5	0	6	1	0	3	13	1	4	0	0	1	0	13	0	1	6
AEB 143	BOT RED 29	41.99 m	0	0	0	1	10	3	0	4	3	0	1	1	2	0	2	17	0	0	5
AEB 142	BOT RED 29	41.64 m	0	0	0	3	11	2	0	8	5	0	2	0	3	3	0	23	0	1	3
AEB 141	TOP WHITE 28	41.39 m	4	0	0	0	13	1	4	4	2	1	2	0	3	0	0	38	0	0	7
AEB 140	MID WHITE 28	41.08 m	2	0	0	0	3	3	0	2	1	1	3	0	7	0	0	13	0	0	4
AEB 139	BOT WHITE 28	40.84 m	3	0	0	1	9	1	1	5	0	0	3	0	2	0	0	20	0	1	6
AEB 138	TOP RED 28	40.32 m	1	0	2	3	11	2	1	5	4	0	2	0	1	1	0	16	0	0	4
AEB 137	MID RED 28	39.96 m	5	0	3	1	5	2	0	4	5	0	2	0	2	0	0	17	0	0	3
AEB 136	MID RED 28	39.66 m	11	0	0	4	4	0	0	3	4	1	1	0	1	2	1	10	0	0	2
AEB 135	BOT RED 28	39.38 m	2	0	0	0	11	0	0	1	2	2	12	0	3	0	0	27	0	0	3
AEB 134	MID WHITE 27	39.15 m	9	0	0	0	10	2	2	2	0	0	3	0	4	3	0	27	0	1	8
AEB 133	MID WHITE 27	38.95 m	2	0	2	2	4	0	0	6	1	0	1	0	5	0	0	40	0	0	9
AEB 132	TOP RED 27	38.81 m	2	0	1	1	4	2	2	4	0	0	2	0	3	1	0	13	0	0	5
AEB 131	TOP RED 27	38.65 m	0	0	2	2	4	0	0	5	2	1	2	0	0	0	1	12	0	0	3
AEB 130	MID RED 27	38.41 m	0	0	0	0	3	0	0	5	3	0	2	0	0	0	0	12	0	0	0
AEB 129	MID RED 27	38.13 m	0	0	2	0	10	2	0	1	2	0	2	0	1	0	0	11	0	0	1
AEB 128	BOT RED 27	37.82 m	4	0	0	2	2	0	0	3	0	0	1	0	0	2	0	1	0	0	3

sample	Lithology	Stratigraphy	Pullenia bulloides	Pullenia quinqueloba	Rectuvigerina multicostata	Reussella sp.	Rosalina sp.	Sigmavirgulina tortuosa	Sigmoilopsis schlumbergeri	Siphonina reticulata	Sphaeroidina bulloides	Spiroloculina sp.	Stilostomella sp.	Textularia sp.	Trifarina bradyi	Trifarina carinata	Uvigerina pigmea	Uvigerina semiornata	Valvulineria sp.	not identified	Total benthic
AEB 269	MID RED 44	71.28 m	1	5	1	0	1	0	0	10	8	2	1	7	1	10	1	0	1	1	288
AEB 266	MID WHITE 43	70.18 m	9	5	2	0	0	0	0	11	7	0	5	2	6	6	8	27	0	0	479
AEB 264	BOT WHITE 43	69.82 m	7	0	0	0	2	0	0	1	7	0	2	2	1	6	3	2	1	1	230
AEB 262	MID RED 43	69.20 m	1	1	0	0	0	0	0	1	8	0	1	2	58	0	5	0	0	0	235
AEB 259	BOT RED 43	68.50 m	6	5	0	0	0	0	0	2	24	1	5	7	172	2	19	5	3	2	637
AEB 257	MID WHITE 42	67.99 m	7	2	0	0	1	0	0	8	12	2	4	3	20	0	18	0	0	0	385
AEB 256	BOT WHITE 42	67.56 m	5	1	0	0	0	0	0	3	4	0	1	2	4	2	6	0	0	0	231
AEB 254	MID RED 42	66.80 m	1	3	1	0	1	0	2	5	23	0	1	3	3	3	12	0	0	0	393
AEB 252	BOT RED 42	66.19 m	5	3	0	0	0	0	0	2	8	1	1	2	6	5	6	0	0	0	295
AEB 248	MID WHITE 41	64.90 m	13	5	2	0	0	0	1	3	7	1	8	0	4	4	4	0	2	0	279
AEB 210	TOP WHITE 34	53.38 m	4	2	0	0	0	0	0	2	5	1	1	0	0	8	11	0	0	0	199
AEB 209	MID WHITE 34	53.19 m	5	1	0	0	1	0	2	3	4	4	1	1	0	4	40	0	1	0	274
AEB 208	BOT WHITE 34	53.04 m	3	1	0	0	1	0	2	2	3	3	1	0	0	5	64	0	0	0	198
AEB 207	TOP RED 34	52.63 m	6	1	1	0	0	0	2	2	8	2	2	1	0	7	102	0	0	0	338
AEB 206	MID RED 34	52.36 m	7	3	0	0	0	0	1	3	19	0	3	5	1	9	50	0	2	1	350
AEB 205	MID RED 34	52.12 m	3	5	0	0	0	1	2	5	20	0	3	0	1	1	47	0	0	0	307
AEB 204	BOT RED 34	51.88 m	6	1	2	0	3	0	3	4	6	3	2	1	0	7	56	0	0	1	296
AEB 203	TOP WHITE 33	51.27 m	2	1	1	0	0	0	2	0	8	2	2	0	0	6	32	0	0	0	277
AEB 202	MID WHITE 33	50.88 m	2	2	0	0	1	0	1	3	3	1	2	0	0	9	29	0	0	0	244
AEB 201	BOT WHITE 33	50.58 m	2	1	0	0	0	0	0	3	8	0	1	1	1	7	30	0	1	1	232
AEB 200	TOP RED 33	50.29 m	4	1	0	0	0	0	1	2	8	0	6	1	0	2	72	0	0	0	285
AEB 199	MID RED 33	49.88 m	4	6	0	0	0	0	1	0	15	1	1	2	0	3	92	0	0	0	358
AEB 198	MID RED 33	49.34 m	0	6	0	0	0	1	1	1	13	1	0	6	0	8	81	0	0	1	417
AEB 197	MID RED 33	48.75 m	1	5	0	0	0	2	3	4	18	0	2	3	1	15	19	0	0	0	214
AEB 196	BOT RED 33	48.30 m	3	5	0	0	0	0	2	4	8	1	3	2	4	5	67	0	0	2	267
AEB 171	TOP WHITE 32	48.00 m	3	0	1	0	1	0	1	2	4	1	1	1	6	7	37	1	0	0	200
AEB 170	MID WHITE 32	47.87 m	8	1	1	0	0	0	0	15	11	1	1	2	7	11	80	0	0	0	414
AEB 169	BOT WHITE 32	47.75 m	4	3	3	0	0	0	0	3	8	0	3	0	2	8	56	0	0	0	211
AEB 168	TOP RED 32	47.54 m	0	3	0	0	0	0	1	0	10	1	0	3	3	3	105	0	0	1	253
AEB 167	MID RED 32	47.26 m	3	0	0	0	0	0	2	0	11	2	0	0	2	1	93	0	1	0	287
AEB 166	MID RED 32	46.95 m	3	3	1	0	0	2	1	1	9	5	1	2	6	9	46	0	0	1	216
AEB 165	BOT RED 32	46.78 m	5	0	1	1	0	0	1	5	10	1	0	3	1	9	74	1	0	0	278
AEB 150	TOP WHITE 29	43.86 m	0	0	1	0	0	0	0	1	6	0	0	0	2	8	12	2	0	0	204
AEB 149	MID WHITE 29	43.68 m	0	0	0	0	1	0	0	4	4	0	2	0	4	9	18	4	0	0	269
AEB 148	BOT WHITE 29	43.42 m	1	3	1	0	0	0	1	1	2	0	1	0	2	1	15	2	0	1	188
AEB 147	TOP RED 29	43.11 m	2	3	0	0	0	0	2	1	2	1	1	2	1	2	88	2	1	0	297
AEB 146	TOP RED 29	42.78 m	3	4	0	0	0	0	2	0	7	3	0	0	0	2	93	0	1	1	267
AEB 145	MID RED 29	42.52 m	2	3	0	0	0	0	1	0	9	5	0	2	1	1	146	1	2	3	386
AEB 144	MID RED 29	42.21 m	1	0	0	0	0	0	4	0	3	3	1	0	2	1	122	1	0	1	315
AEB 143	BOT RED 29	41.99 m	1	1	1	0	0	1	1	0	6	5	3	1	0	2	30	1	0	0	205
AEB 142	BOT RED 29	41.64 m	2	5	0	0	1	0	4	3	4	3	1	1	2	8	34	2	1	0	270
AEB 141	TOP WHITE 28	41.39 m	2	6	0	0	0	0	0	1	12	2	1	0	0	3	53	4	0	0	282
AEB 140	MID WHITE 28	41.08 m	4	1	1	0	0	0	0	4	8	1	2	0	4	10	28	2	0	1	217
AEB 139	BOT WHITE 28	40.84 m	2	1	0	0	1	2	1	1	8	0	5	0	3	5	30	4	1	1	211
AEB 138	TOP RED 28	40.32 m	3	2	0	0	0	0	2	0	5	0	3	1	1	1	28	3	0	1	191
AEB 137	MID RED 28	39.96 m	1	0	0	3	1	0	1	1	4	2	1	2	2	4	25	0	1	0	220
AEB 136	MID RED 28	39.66 m	2	1	2	1	0	5	2	1	3	3	2	0	14	11	41	4	1	1	350
AEB 135	BOT RED 28	39.38 m	4	2	0	0	0	2	3	2	6	1	1	0	1	8	27	5	0	0	261
AEB 134	MID WHITE 27	39.15 m	2	4	0	0	0	0	0	9	3	3	3	0	9	5	27	7	0	0	326
AEB 133	MID WHITE 27	38.95 m	4	1	1	0	0	1	2	9	9	0	1	0	1	9	34	10	0	4	322
AEB 132	TOP RED 27	38.81 m	2	1	0	1	0	0	0	10	2	2	2	0	5	5	29	6	0	0	221
AEB 131	TOP RED 27	38.65 m	1	1	0	0	0	0	3	5	9	1	2	0	0	8	84	5	2	3	266
AEB 130	MID RED 27	38.41 m	2	0	0	0	1	0	2	1	6	0	2	0	0	6	73	0	0	0	229
AEB 129	MID RED 27	38.13 m	1	7	0	0	1	0	3	2	8	0	2	0	0	5	70	1	1	2	260
AEB 128	BOT RED 27	37.82 m	0	1	3	0	0	8	3	0	2	1	1	1	0	10	14	1	4	3	190